Self-excitation process due to local seismic amplification responsible for the reactivation of the Salcito landslide (Italy) on 31 October 2002

Francesca Bozzano, Luca Lenti, Salvatore Martino, Antonella Paciello, Gabriele Scarascia Mugnozza

Self-excitation process due to local seismic amplification responsible for the reactivation of the Salcito landslide (Italy) on 31 October 2002

F. Bozzano,[1] L. Lenti,[2] S. Martino,[1] A. Paciello,[3] and G. Scarascia Mugnozza[1]

Received 31 July 2007; revised 25 April 2008; accepted 8 July 2008; published 21 October 2008.

[1] An integrated numerical and geophysical approach was used to investigate the role of local seismic amplification in the reactivation of the Salcito landslide (Italy) after the Molise earthquake of 31 October 2002. Numerical stress-strain analysis with FLAC 5.0 FDM software, performed in dynamic configuration, showed that the 1 Hz frequency was consistent with landslide instability conditions. The Fourier spectrum of the triggering earthquake showed two main peaks occurring at 1 and 2 Hz, respectively, which could be related to local effects. The analysis of H/V spectral ratios of ambient noise records obtained in the landslide area, evidenced amplification effects in the 1–3 Hz range. On the basis of an engineering geology model, numerical modeling of both 1-D and 2-D seismic wave propagation was conducted using linear and nonlinear solutions. The simulation outputs showed (1) a 1 Hz amplification ascribable to 2-D effects due to a landslide mass lying within a basin-like geological structure; (2) a double-peak amplification at about 2 and 3 Hz, respectively, ascribable to 1-D resonance of the landslide mass; and (3) 1-D plus lateral wave effects within the landslide mass in the 2.5–3.5 Hz frequency range. These findings suggest that local amplification of ground motion by the Salcito landslide mass may generate a self-excitation process responsible for its reactivation.

Citation: Bozzano, F., L. Lenti, S. Martino, A. Paciello, and G. Scarascia Mugnozza (2008), Self-excitation process due to local seismic amplification responsible for the reactivation of the Salcito landslide (Italy) on 31 October 2002, *J. Geophys. Res.*, *113*, B10312, doi:10.1029/2007JB005309.

1. Introduction

[2] Seismically induced landslides are documented for some historical earthquakes, such as the 1783 earthquake in Calabria, Italy [*Sarconi*, 1784; *Istituto Nazionale di Geofisica*, 2000], and the 1786 earthquake in Kanding-Luding, China [*Dai et al.*, 2005]. A large database of earthquake-induced landslides for recent earthquakes is available in the literature [*Keefer*, 1984; *Rodriguez et al.*, 1999]. Landslides are one of the most damaging collateral hazards associated with earthquakes. Damage from seismically induced landslides and other ground failures (i.e., cracks along faults, liquefaction, densification) has sometimes exceeded damage from ground shaking, as testified by a recent review of economic losses due to earthquakes [*Bird and Bommer*, 2004].

[3] Some methods have been proposed in the scientific literature for evaluating earthquake-induced landslide hazards at regional scale [*Wieczorek et al.*, 1985; *Wilson and Keefer*, 1985; *Keefer and Wilson*, 1989; *Harp and Wilson*, 1995; *Jibson et al.*, 1998; *McCrink and Real*, 1996; *Jibson et al.*, 2000]. These methods have thus made it possible to single out the most landslide-prone areas and the critical aspects of scenarios of quasi-simultaneous seismic triggering of landslides. Nevertheless, it is only in the past few years that some research has focused on reconstructing the mechanisms of seismically induced landslides and on deterministic prediction of earthquake-induced ground failure scenarios in specific case studies [*Wasowski and Del Gaudio*, 2000; *Havenith et al.*, 2002, 2003a, 2003b; *Bozzano et al.*, 2004b; *Bonci et al.*, 2004; *Martino and Scarascia Mugnozza*, 2005; *Gerolymos and Gazetas*, 2007].

[4] Factors conducive to seismic triggering of landslides encompass local seismic response effects due to the impedance contrast between the bedrock and landslide deposit [*Borcherdt*, 1970; *Nakamura*, 1989], topographical effects [*Chavez-Garcia et al.*, 1997] and trapped wave modes in fault zone areas [*Li et al.*, 1990; *Li and Vidale*, 1996; *Rovelli et al.*, 2002; *Martino et al.*, 2006].

[5] This paper reports on an integrated geophysical and engineering geological approach used to investigate the Salcito landslide, reactivated by the 2002 Molise (Italy) earthquake [*Bozzano et al.*, 2004b] (Figure 1a). This approach includes an analysis of the role of local seismic amplification (from seismometric records and 1-D and 2-D seismic wave propagation models) in seismically induced displacements occurring in existing landslide masses.

2. State of the Art

[6] Worldwide experiences demonstrate that earthquake-induced landslides affect both rock masses and coherent or

[1]Department of Earth Sciences, Research Centre for Geological Risks, University of Rome "Sapienza," Rome, Italy.
[2]LCPC, Paris, France.
[3]ENEA, Santa Maria di Galeria, Rome, Italy.

0148-0227/08/2007JB005309$09.00

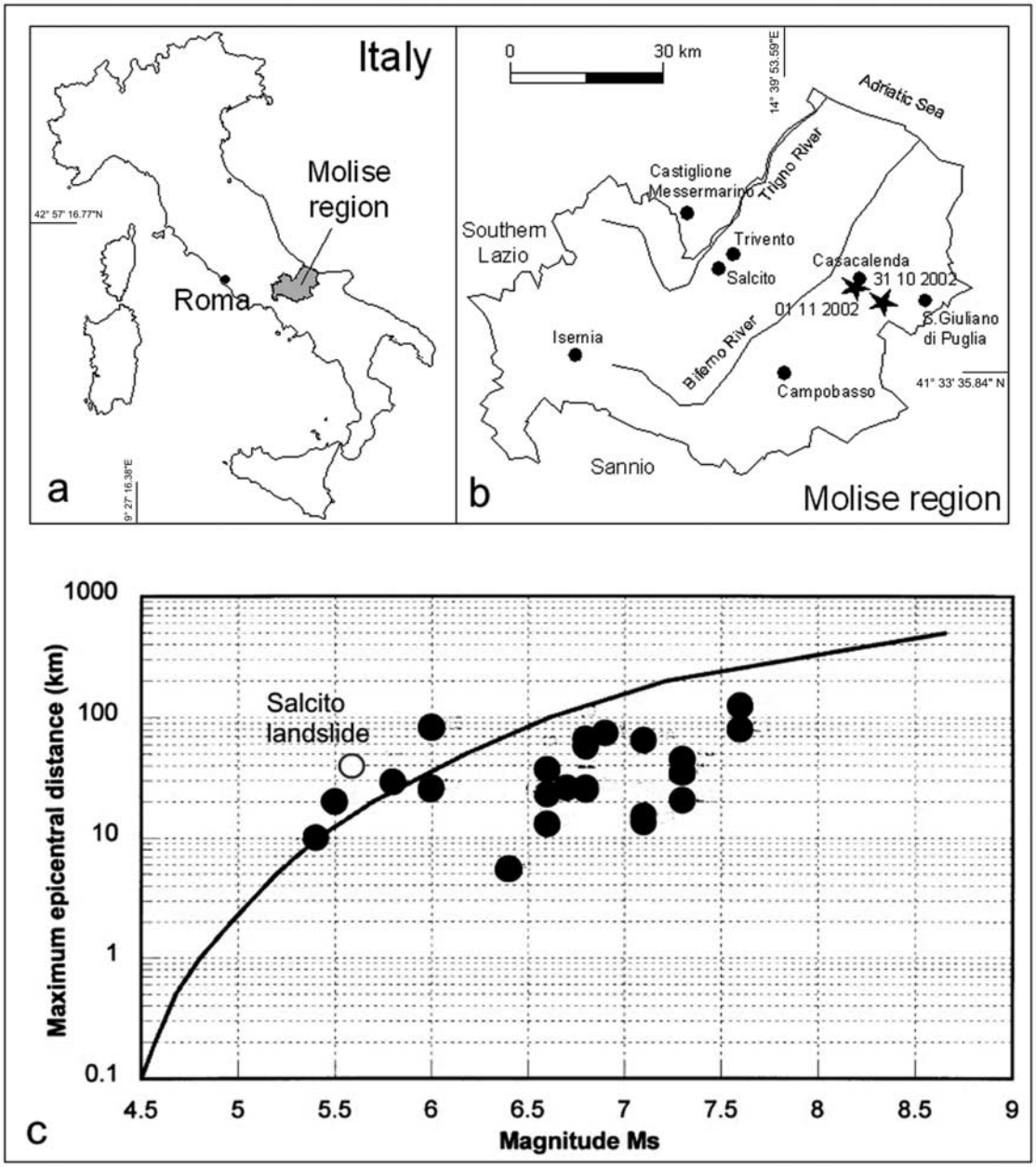

Figure 1. (a) Location of the Molise region; (b) location of the Salcito village and of the Molise earthquake main shocks; (c) maximum epicentral distance versus magnitude (Ms) for seismically induced triggering of coherent landslides (modified from *Rodriguez et al.* [1999]).

granular soils in different ways [*Keefer*, 1984; *Hutchinson*, 1987; *Sassa*, 1996; *Rodriguez et al.*, 1999; *Luzi and Pergalani*, 2000; *Prestininzi and Romeo*, 2000; *Sassa et al.*, 2005]. By collecting and analyzing seismically induced landslide data at global scale, empirical relationships have been established between landslide occurrence and characteristics of the inducing earthquake, such as epicentral distance and magnitude [*Keefer*, 1984; *Ambraseys and Srbulov*, 1995; *Rodriguez et al.*, 1999]. Moreover, pseudodynamic analysis at regional scales has permitted the development of earthquake-triggered landslide scenarios [*Faccioli*, 1995; *Luzi and Pergalani*, 1996; *Romeo*, 2000].

[7] A key relationship is that between the epicentral distance of the landslide and the magnitude of the triggering earthquake. The maximum epicentral distance of a seismically induced landslide may be estimated through magnitude-dependent relations for each type of landslide [*Keefer*, 1984]. Nevertheless, these relations may be altered by local site conditions (tectonic features, stratigraphic conditions, morphology), which amplify the seismic input [*Havenith et al.*, 2003a, 2003b].

[8] The scientific literature offers few papers on the mechanism of earthquake-induced landslides in natural clayey slopes. The reported case histories chiefly refer to the 1964 Alaskan earthquake (M_S = 8.5), which triggered

the Turnagain Heights [*Seed and Wilson*, 1967] and the Fourth Avenue [*Seed*, 1968] landslides. The failure mechanism of these landslides, initially attributed to liquefaction of sandy layers, was subsequently interpreted in terms of progressive degradation of the undrained strength of the local clays [*Stark and Contreras*, 1998]. More recently, two landslides were induced in clayey slopes by the 1988 Saguenay earthquake in Canada (MS = 5.9) [*Lefebvre et al.*, 1992]. As these landslides occurred at considerable distance (about 175 km) from the triggering earthquake, local amplification was supposed to have played a critical role in landslide initiation.

[9] Among available case histories, noteworthy analyses of failure mechanisms for earthquake-induced landslides in natural slopes include the 1980 Irpinia earthquake [*Hutchinson and Del Prete*, 1985; *D'Elia et al.*, 1986; *Martino and Scarascia Mugnozza*, 2005], the 1989 Loma Prieta earthquake [*Seed et al.*, 1991; *Keefer*, 1998], the 1994 Northridge earthquake [*Norton et al.*, 1994], the 1995 Kobe earthquake [*Sassa et al.*, 1996; *Gerolymos and Gazetas*, 2007], the 1997 Umbria-Marche earthquake [*Bozzano et al.*, 2001], the 1999 Kokaeli earthquake [*Bardet and Seed*, 2000; *Cetin et al.*, 2004], the 2001 El Salvador earthquake [*Evans and Bent*, 2004], the 2002 Palermo earthquake [*Bonci et al.*, 2004], and the 2002 Molise earthquake [*Bozzano et al.*, 2004b; *Bianchi Fasani et al.*, 2004].

[10] A reliable back analysis of earthquake-induced landslides depends on adequate knowledge of the cyclical response of the soil to a wide range of shear strains. Indeed, assessing shear strains often requires understanding soil stiffness and damping in a nonlinear field. This is particularly true for clay shales, for which experimental knowledge is poor [*D'Elia*, 1983; *Olivares*, 1996; *Olivares and Silvestri*, 2001] and does not provide a comprehensive picture of the stress-strain behavior of these materials upon shaking. Available literature suggests that (1) stiffness and damping, as well as linear and volumetric thresholds of shear strains (which relate low-elastic, middle-plastic and large-plastic shear strain ranges), are influenced by the mesostructural properties of these soils, rather than by plasticity of each clay fragment, and (2) nonlinear behavior is notable even at small-to-medium strain levels [*Lanzo*, 1993]. Reduction in stiffness and increase in damping ratio with shear strain may significantly constrain both the displacement field within a slope and local amplification phenomena, as they strictly depend on the characteristics of the materials in which seismic waves propagate. The study covered by this paper assumes that local amplification of ground motion can promote landslide reactivation.

[11] Since the end of the 1980s, several methodologies have been developed to evaluate local seismic effects. Analysis of the spectral ratio between the vertical and horizontal components of microtremors (ambient noise of natural or human origin) is a widely applied technique, given its low cost and speed of use [*Lachet et al.*, 1995]. This technique was proposed by *Nakamura* [1989] to assess amplification in a site with distinctive geological conditions (e.g., sedimentary layer overlapping a homogeneous semispace and high impedance contrast between the two formations). Assuming that the vertical component of motion is not significantly amplified by the surface layer, its deconvolution from the horizontal component (corresponding to the H/V spectral ratio in the frequency domain) provides an estimate of the 1-D resonance frequency. Nevertheless, 3-D amplification effects due to trapped modes within fault zones [*Martino et al.*, 2006] or topographic site effects [*Chavez-Garcia et al.*, 1996, 1997] have also been detected through the H/V methodology. Obviously, this methodology cannot identify amplification phenomena that equally involve the horizontal and vertical components of ground motion.

[12] Better information can be obtained from local velocity or acceleration records of seismic events (where available) after removing the effects due to the source and wave propagation. This is usually done using the approach proposed by *Borcherdt* [1994], which takes into account the ratio of the Fourier spectra of the records obtained at the site to the spectra of the records of the same event obtained in a representative "reference station".

[13] However, this methodology needs planning and deploying seismic arrays, which should operate long enough to produce an appropriate number of records; therefore, the methodology can only be applied in sites having an adequate level of seismic activity.

[14] Up to now, methodologies of analysis of local seismic response have rarely been employed in the study of both seismic triggering of landslides and site amplification in landslide areas. In the past few years, some experiments in this area have been conducted by *Havenith et al.* [2003a, 2003b] in Kyrgyzstan, on rock avalanche deposits, and in Italy on two Central Apennine areas with widespread landslide phenomena and high seismic hazard [*Del Gaudio and Wasowski*, 2004; *Bordoni and the Cavola Experiment Team*, 2005]. To investigate slope stability in response to a seismic input and, above all, to quantify coseismic and postseismic displacements, different techniques have been developed since the 1960s. *Newmark* [1965] attempted to evaluate coseismic displacements via pseudostatic analysis based on landslide acceleration exceeding a given critical threshold. *Ambraseys and Srbulov* [1995] evaluated postseismic displacements by means of a pseudostatic approach, which cumulated the displacements due to residual inertial forces acting on a rigid and geometrically regular landslide mass. In the study of coseismic and postseismic slope deformations, dynamic analyses with FEM and FDM software may benefit from time-dependent force analysis; the latter takes into consideration both inertial effects due to landslide mass movement and shaking effects due to the seismic input [*Martino and Scarascia Mugnozza*, 2005]. In these numerical approaches, many parameters are to be defined and evaluated after selecting the constitutive laws governing stress-strain relations in the investigated soils. So far, no specific solutions have been offered for cohesive and stiff materials, whose nonlinear behavior should be taken into account. Some numerical codes (i.e., FLAC 5.0 [*ITASCA Consulting Group*, 2005]), however, permit a time-dependent nonlinear incremental solution where dynamic properties (i.e., shear stiffness and damping) decay with shear strain.

3. The Salcito Landslide

3.1. Seismicity of the Salcito Area

[15] The Salcito landslide area (Figure 1a) has no local seismicity, as demonstrated by the location of the seismic

events reported in the Italian CPTI04 catalog [*Istituto Nazionale di Geofisica e Vulcanologia*, 2004; *Gruppo di Lavoro*, 2004]. Nevertheless, seismic sources lying at distances of 30–50 km from the site (Sannio, southern Abruzzo) can produce events of high magnitude (of up to 7).

[16] Available macroseismic data [*Istituto Nazionale di Geofisica e Vulcanologia*, 2000; *Castello et al.*, 2005; *Istituto Nazionale di Geofisica e Vulcanologia*, 2004; G. Monachesi and M. Stucchi, DOM4.1 un catalogo parametrico di terremoti di area italiana al di sopra della soglia di danno, 1997, http://emidius.mi.ingv.it/DOM/home.html; Istituto Nazionale di Geofisica e Vulcanologia, Database Macrosismico Italiano, 2004, available at http://emidius.mi.ingv.it/DBMI04], most of which come from the neighboring village of Trivento, reveal that the historically highest intensity at the site [*Sieberg*, 1930] was associated with the Bojano earthquake (epicentral intensity X MCS); the earthquake occurred at a distance of about 30 km from Salcito on 26 July 1805. Considering the effects of this event at Trivento, national catalogs report a felt intensity of VIII MCS, while a specific study [*Esposito et al.*, 1987] estimates an intensity of VII MCS. All the authors agree that the environmental effects induced by the earthquake in the Salcito-Trivento area were severe [*Cara et al.*, 2005].

[17] On 31 October 2002, a moderate earthquake (Ml = 5.4) took place in the Molise region [*Dipartimento della Protezione Civile*, 2004]. The event has remained sadly famous for killing 30 people, mostly children involved in the collapse of the San Giuliano di Puglia primary school. On 1 November, the area was hit by a twin earthquake [*Vallée and Di Luccio*, 2005] occurring about 10 km west of the first one (Figure 1a). The two main shocks and the many aftershocks of the Molise sequence were recorded by the Italian Strong Motion Network, RAN; 196 records were obtained from 51 earthquakes, which occurred between October 2002 and December 2003 and had a magnitude range of 2.6 to 5.4 Ml. The records obtained at Castiglion Messermarino (CMM) [*Dipartimento della Protezione Civile*, 2004] are of particular interest to this study. Indeed, this is the nearest accelerometer station (15 km) to the landslide area. The station, located on a rock site and equipped with a digital data collection unit, recorded the main shocks and three aftershocks with a local magnitude of about 4. Location of the CMM station and analysis of its accelerometer records through the receiver function technique [*Field and Jacob*, 1995] show that the site is not prone to local amplification effects.

3.2. The 31 October 2002 Reactivation of the Salcito Landslide

[18] A few hours after the 31 October earthquake, a landslide developed about 30 km from its epicenter, in the municipality of Salcito, where a local felt intensity of V MCS was assessed (http://www.ingv.it). The earthquake caused a complex ground crack pattern (Figure 2) and downslope displacements of up to 2 m [*Bozzano et al.*, 2004b; *Bianchi Fasani et al.*, 2004], damaging some farmhouses and lifelines. This landslide, which involved an area of about 1 km^2 and an estimated volume of 40 Mm^3, can be classified as an earth slide with a deep planar slip surface [*Bianchi Fasani et al.*, 2004]. No rainfall occurred in the days preceding landslide reactivation. Nevertheless, as discussed later, the landslide mass was saturated owing to groundwater seepage. The Salcito landslide lies beyond the upper bound of the epicentral distance versus magnitude curve proposed by *Rodriguez et al.* [1999] for seismically induced coherent landslides (Figure 1b).

[19] On the basis of interpretation of the observed ground crack distribution and on the reconstructed kinematics, the landslide area may be divided in three zones.

[20] 1. An upslope zone exists with open cracks and extensional deformations, according to a plastic flow model [*Savage and Smith*, 1986; *Savage and Wasowski*, 2006], sand-mud boils and widespread ground settlements. This zone is the active zone of the landslide, where vertical stresses in the landslide mass exceed horizontal ones. This tensional condition favors the opening of cracks and the formation of scarps, generating marked stiffness contrasts between the landslide mass and the adjacent substratum (Figures 2b and 2d).

[21] 2. A large midslope zone with no significant surface effects, except for some low persistent longitudinal ground cracks, is found in the western side, without any indicators of kinematics. This zone represents an extensive neutral zone [*Hutchinson*, 1987], where substantial shear stresses in the horizontal direction cause plug deformations, according to a plastic flow model, along superficial cracks and deep rupture surfaces. This tensional condition, which is likely to be due to a strike mechanism, does not create significant stiffness contrasts inside the landslide mass (Figure 2a).

[22] 3. A downslope zone exists with closed cracks and bulging clay material that do not result from extensional deformations but from major compressive stresses parallel to the slope. After the 31 October reactivation, a wide thrust zone lying in this sector of the slope experienced a number of fissures and disturbances that were associated with radial cracks. This zone is the passive zone of the landslide mass, where horizontal stresses exceed vertical ones. This tensional condition, which is responsible for thrust kinematics, closed cracks (Figure 2c), compression along the rupture surface and water ejection, does not give pronounced stiffness contrasts between the landslide mass and the substratum.

[23] The landslide-affected slope provides ample evidence of prior mass movements, consistent with historical sources [*Pepe*, 1806; *Esposito et al.*, 1987]. As a consequence, the event must be the result of partial or total remobilisation of a previous landslide mass [*Bozzano et al.*, 2004b; *Bianchi Fasani et al.*, 2004]. Actually, significant ground effects have been reported in the Salcito municipality after the above mentioned Bojano earthquake in 1805.

4. Engineering Geology Model of the Salcito Landslide

[24] The Salcito landslide site is located in the Molise section of the Apennine chain. In this sector of the chain, some of the main structural stratigraphic units of the orogenic belt are tectonically juxtaposed: the Sannio pelagic basin unit and the Molise pelagic basin unit [*Patacca et al.*, 1992]. The Salcito landslide developed within the Argille Varicolori Formation of the Sannio Unit (Figure 3). This formation (Oligo-Miocene) is composed of fissured clay shales, locally interlayered with intensely sheared arena-

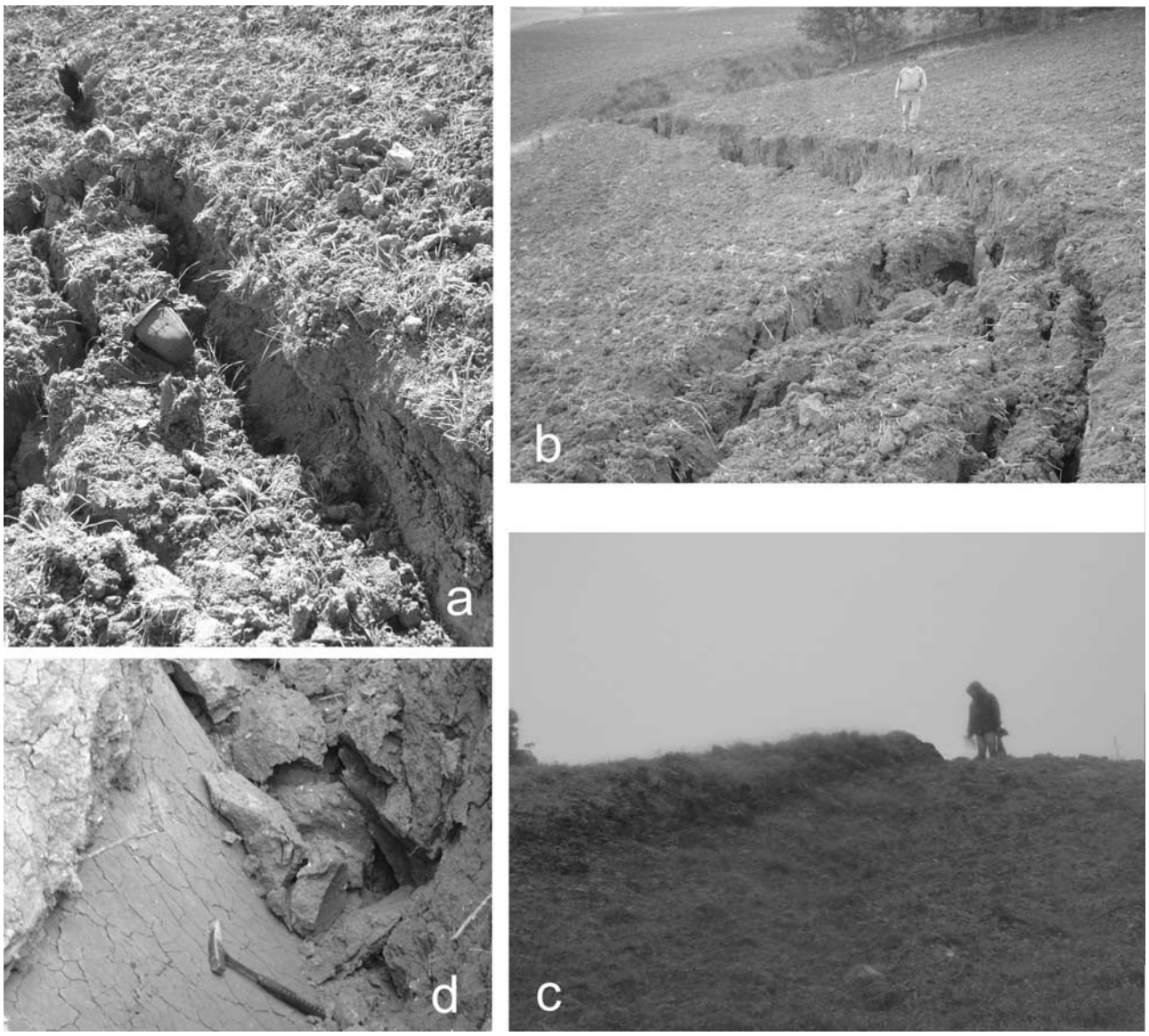

Figure 2. Ground cracks due to the Salcito landslide reactivation of 31 October 2002: (a) strike crack, (b) normal dip-slip crack; (c) detail of secondary scarp; (d) dip-slip compressive crack.

ceous and marly limestone beds (Figure 4b). The upper part of the Sannio Unit, outcropping south of the Salcito village, consists of reddish marls and massive calcarenites, dislodged by a NW-SE multithrust system and by a NE-SW tear-fault system. The early middle Pliocene compressive tectonics produced an E-W trending thrust of the Sannio Unit over the Molise Unit. Starting from the late Pliocene, compressive tectonics has evolved into strike-slip faulting; as a consequence, the thrust front was shifted northward by a NE-SW left-lateral tear fault.

[25] With regard to hydrogeological features, the marly calcarenitic members of the Molise Unit (Tufillo Formation) (Figure 4a) contain an aquifer that is hydraulically confined by the Argille Varicolori aquitard, which belongs to both the Molise and Sannio Units. Along the slope affected by the landslide, a shallow aquifer drains into the Argille Varicolori of the Sannio Unit. The aquifer lies within the first 15 m below ground level (bgl); the groundwater table is located about 1 m bgl [*Bozzano et al.*, 2004b].

[26] The main crown in the detachment zone of the landslide, observed after the seismically induced reactivation, lies close to one of the main strike-slip faults. Two boreholes (S1 and S2 in Figure 3) were drilled (60 m) into the landslide mass in March–July 2003 [*Bianchi Fasani et al.*, 2004] (see geological section in Figure 3). In detail, the stratigraphic log indicates that the main deep sliding surface lies at a maximum depth of 50 m bgl and that it comprises secondary sliding surfaces. Silty-clayey soil with evidence of water flow (i.e., nodular concretions, oxidized levels) was found at 0 to 15 m bgl; this finding is consistent with hydrogeological observations at the surface. Medium-consistency clay shales were detected down to 30 m in S2 and down to 50 m in S1 (Figure 5a). Typical evidences of sliding surfaces were noted at about 30 m bgl in S2 and at about 50 m bgl in S1: intensely brecciated levels (Figure 5b),

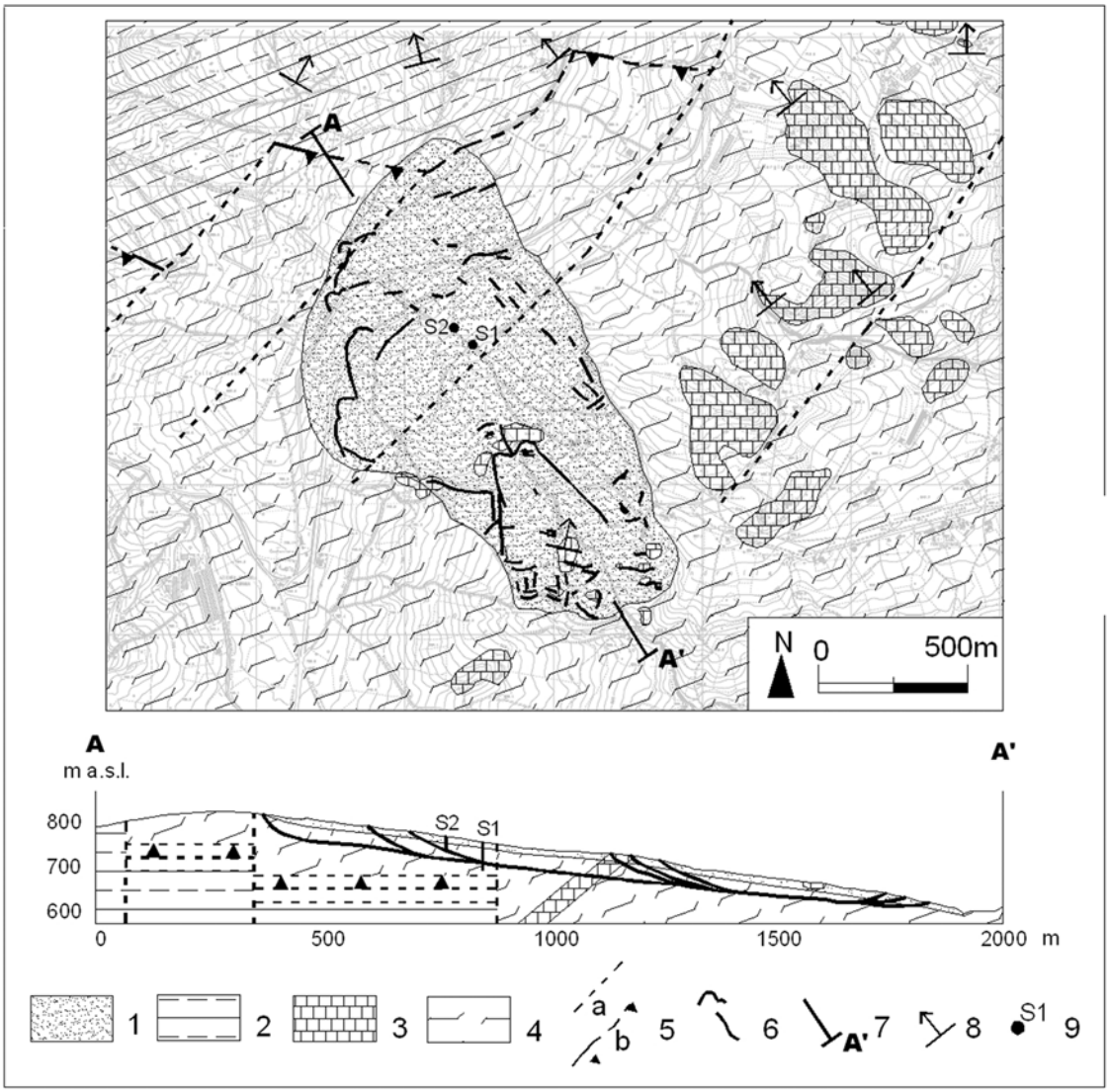

Figure 3. Geological sketch of the Salcito landslide area: 1, landslide mass; 2, marls with calcarenites (Tufillo Formation); 3, calcarenites and marls of the Sannio Unit; 4, fissured clay shales (Argille Varicolori Formation of the Molise Unit); 5, tear fault (a), thrust (b); 6, ground crack observed after the Salcito landslide reactivation of 31 October 2002; 7, trace of geological section; 8, attitude of beds; 9, borehole.

oxidation phenomena within the clay shale mass and sharp changes in water content [*Bozzano et al.*, 2004b]. On the basis of stratigraphic evidence, a deeper artesian aquifer at 30 m bgl was also assumed.

[27] The clay shales sampled in the boreholes were geotechnically characterized, statically and dynamically, via Static Triaxial Tests (CIU), Resonant Column and Cyclic Torsional Shear tests. Additionally, a downhole and a cross-hole test for both P wave and S wave velocities were performed in the S1 and S2 boreholes, respectively [*Bozzano et al.*, 2004a]. Figure 6 displays the shear stiffness and damping decay curves from the above cyclical laboratory tests.

5. Dynamic Numerical Modeling

[28] Dynamic stress-strain analysis (2-D numerical modeling) was carried out with the FLAC 5.0 [*ITASCA Consulting Group*, 2005] FDM software. The analysis was intended to elucidate the role of seismic input, in terms of both amplitude and frequency, in landslide triggering. For the numerical model, a 154 $\times$ 59 mesh with a 10 m square resolution was used, assuming an infinite slope geometry [*Guadagno et al.*, 2003]. The model is composed of three strata with a lower boundary parallel to the slope surface (Figure 7). This hypothesis is consistent with the engineering geology model obtained for the landslide (Figure 3), as well as with the large neutral zone, responsible for the main observed translational component of the sliding mechanism.

[29] An elastic-perfectly plastic Mohr-Coulomb constitutive law was attributed to all of the simulated materials. Moreover, both x displacements and y displacements were permitted along the lateral boundaries of the model. Adopting an infinite slope model, a stationary ground flow parallel to the slope was also simulated within the upper 15 m deep remolded clay.

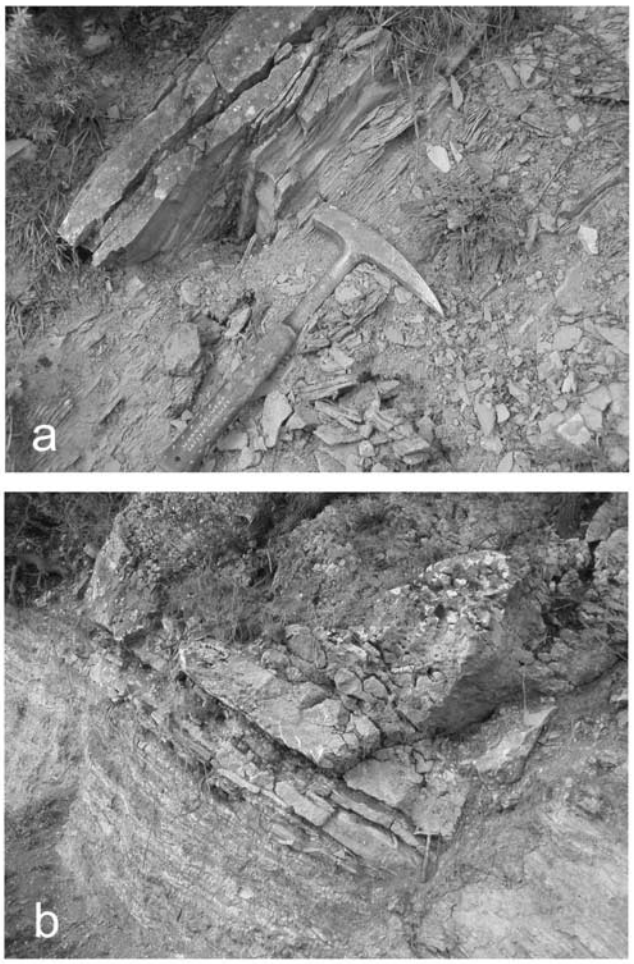

Figure 4. (a) Outcropping marls with calcarenites of the Tufillo Formation; (b) outcropping calcarenites and marls of the Sannio Unit.

[30] Physical and mechanical parameter values were derived from both laboratory tests and field geophysical investigations [*Bozzano et al.*, 2004a], taking into account their variation with in situ confining pressures (Table 1). Initial equilibrium was obtained under the action of gravity only. During dynamic modeling, geotechnical deformational parameters were modified taking into account the decay of the G/G_0 ratio (dynamic shear modulus/constant dynamic shear modulus at low strains) versus the shear strain from dynamic laboratory tests (Figure 6). Mechanical dissipation was computed using a Rayleigh Damping function, adding a mass-dependent term to a stiffness-dependent one in the following form:

$$C = \alpha M + \beta K \tag{1}$$

where α is constant for the mass damping (M) and β is constant for the stiffness damping (K). This dissipation function implies a minimum frequency in the form

$$\left(\omega_{\min} = (\alpha/\beta)^{1/2}\right) \tag{2}$$

which gives the minimum damping in the following form:

$$\left(\xi_{\min} = (\alpha\beta)^{1/2}\right) \tag{3}$$

The damping $\xi_{\min}$ values were modified during dynamic simulation according to the laboratory curves of D/D_0 (damping/constant damping at low strains) versus shear strain (Figure 6).

[31] For numerical modeling, equivalent dynamic inputs were defined as sinusoidal functions with (1) amplitude from 0.1 to 0.01 m/s^2, consistent with the actually recorded PGA value (about 0.05 m/s^2); (2) frequency values of 1 and 2 Hz, observed in the Fourier spectrum of the record obtained at the CMM station from the 31 October main shock (these frequencies are consistent with the geometric resolution of the grid, according to the maximum admissible

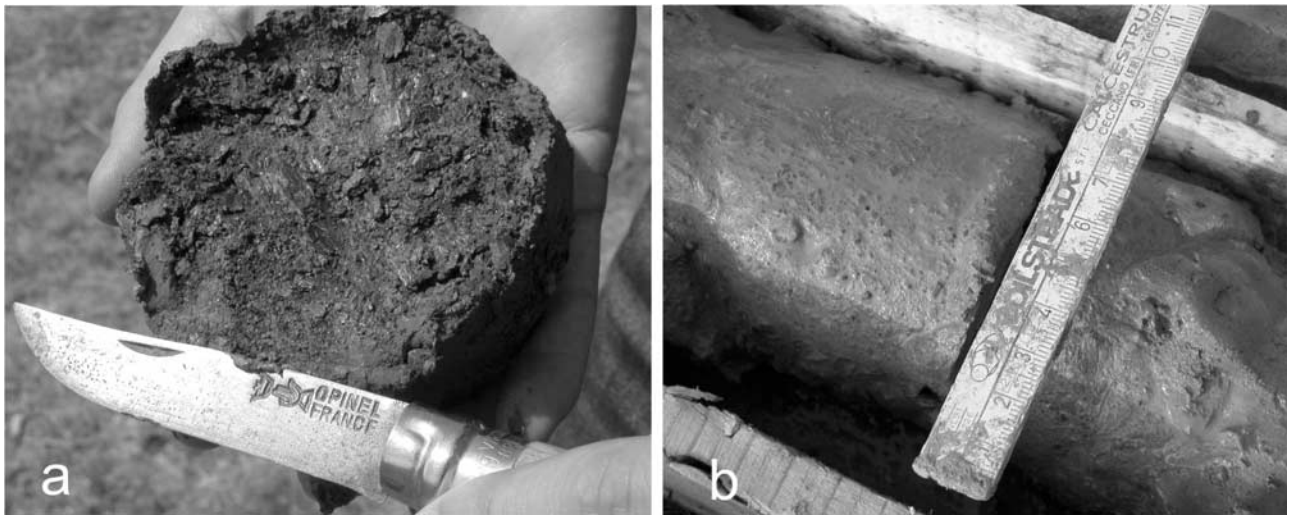

Figure 5. (a) Clay shales of the Argille Varicolori Formation within the landslide mass and (b) rupture surface of the Salcito landslide, sampled in the S1 borehole.

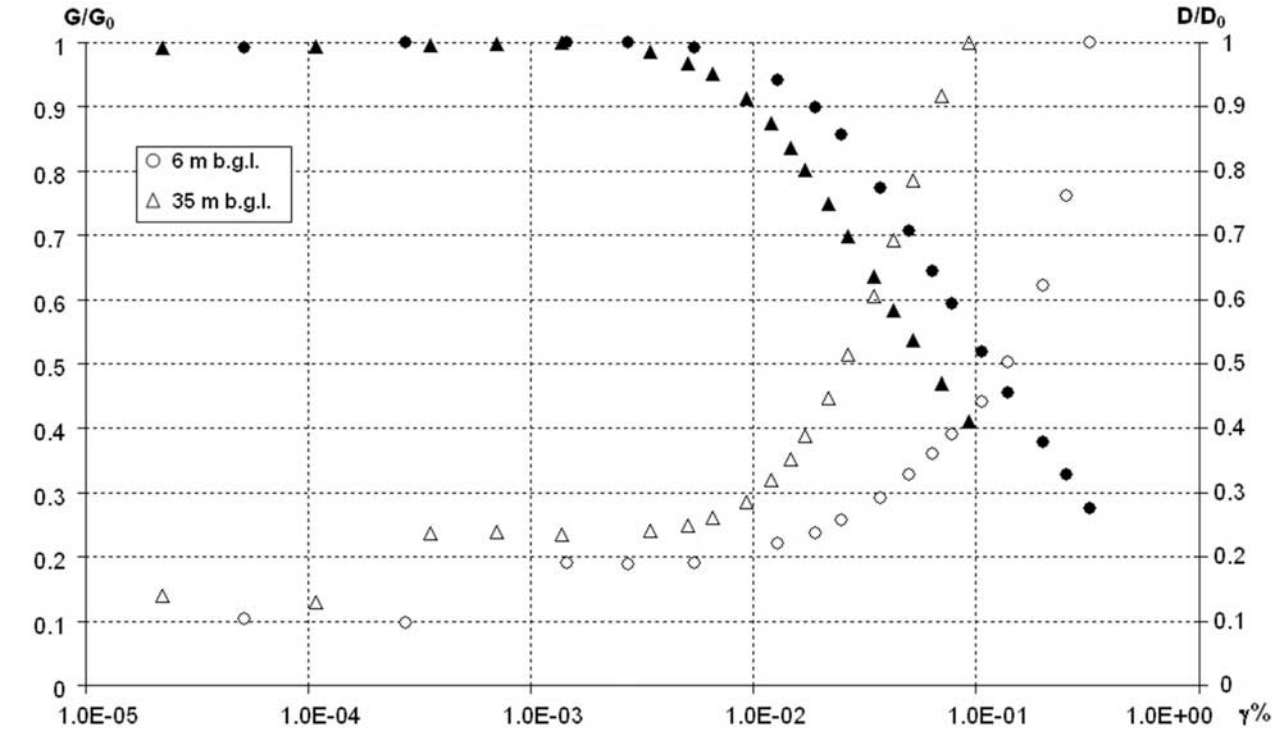

Figure 6. Normalized dynamic shear modulus G/G_0 (filled symbols) and normalized damping D/D_0 (empty symbols) versus percentage cyclic shear strain (γ%), obtained from resonant column laboratory tests.

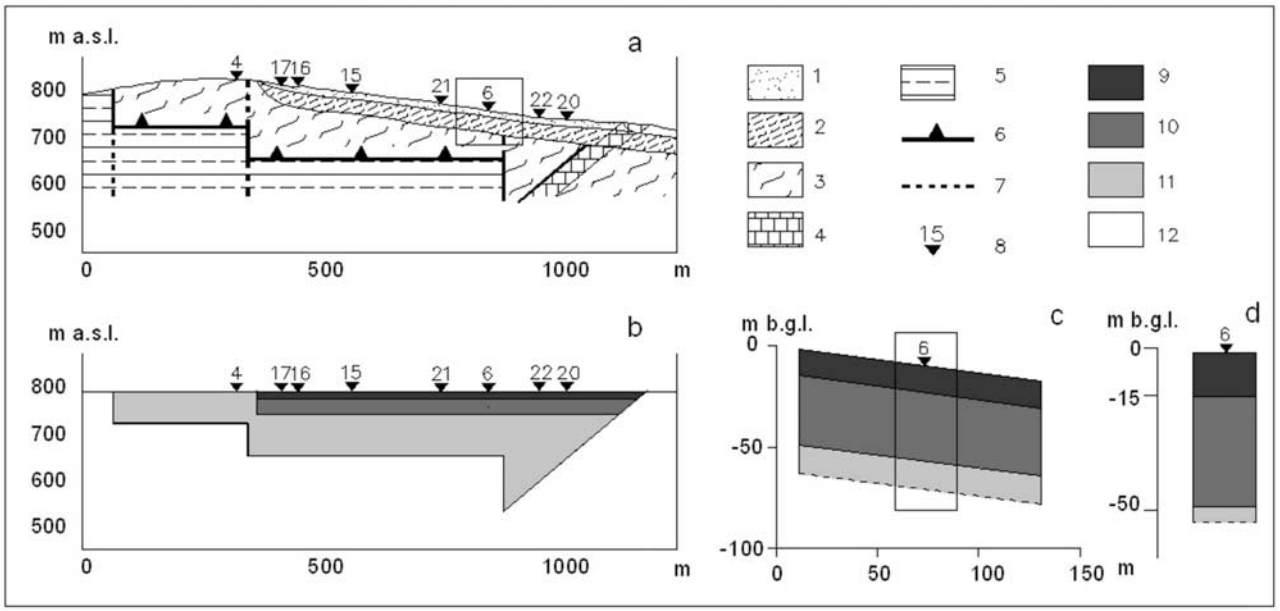

Figure 7. Model project for local seismic response simulations: (a) simulated geological section (the rectangular area is zoomed in Figure 7c); (b) numerical 2-D model (INGV-WISA) along section AA' of Figure 3; (c) numerical 2-D model (FLAC 5.0) (the rectangular area is zoomed in Figure 7d); (d) numerical 1-D model (SHAKE). Key to legend: 1, 15 m thick remolded clays within the landslide mass; 2, softened clay shales within the landslide mass; 3, fissured clay shales of the Argille Varicolori Formation; 4, calcarenites with marls of the Sannio Unit; 5, marls with calcarenites of the Tufillo Formation; 6, thrust; 7, tear fault; 8, noise recording station; 9, 15 m thick remolded clays within the landslide mass (B1a); 10, softened clay shales within the landslide mass (B1b); 11, fissured clay shales of the Argille Varicolori Formation (B2); 12, calcarenites with marls of both the Sannio Unit and the Tufillo Formation (bedrock).

Table 1. Parameter Values Used for Numerical Simulations[a]

	Depth (m bgl)	Density (kg/m^3)	Et[b] (Pa)	Es[b] (Pa)	ν	ϕ (deg)	c (Pa)	ten (Pa)	k (m/s)	$G_{0\ dyn}$ (Pa)	V_s (m/s)	D_0 (%)
Remoulded clays	0–15	2100	$172.37\sigma_3 + 8.00E+07$	$74.26\sigma_3 + 2.00E+06$	0.25	17	0	0	1.00E − 08	4.79E + 07	178	5
Softened clay shales	15–50	2100	$172.37\sigma_3 + 8.00E+07$	$74.26\sigma_3 + 2.00E+06$	0.25	17	0	0	1.00E − 08	2.20E + 08	341	5
Shear zone	50–52	2100	$387.64\sigma_3 + 1.00E+06$	$40.61\sigma_3 + 3.34E+05$	0.25	17	0	0	1.00E − 11	2.20E + 08	341	5
Clay shales	52–200	2200	$172.37\sigma_3 + 8.00E+07$	$74.26\sigma_3 + 2.00E+06$	0.25	22	2.30E + 04	5.70E + 04	1.00E − 09	4.79E + 09	990	5

[a]Et, elastic Young modulus, Es, elastoplastic secant modulus (according to *Bozzano et al.* [2006]); ν, Poisson ratio; ϕ, internal friction angle; c, cohesion; ten, tension cutoff; k, permeability coefficient; G_{0dyn}, dynamic elastic modulus; V_s, S wave velocity; D_0, elastic damping.
[b]Static triaxial modulus versus confining pressure (σ_3) in the range 1.00E + 05 − 7.50E + 05 Pa.

frequency of the model $f = V_s/10\Delta l$ [*Kuhlemeyer and Lysmer*, 1973], where V_s is the velocity of S waves and Δl is the size of the largest mesh of the grid); (3) three representative cycles, evaluated from the magnitude of the earthquake [*Seed and Idriss*, 1969; *Seed*, 1979; *Martino and Scarascia Mugnozza*, 2005; *Martino et al.*, 2007]; and (4) input duration obtained from frequency and number of representative cycles. This allows new static conditions to be reached; a simulation time longer than the input one was selected.

[32] The following two conditions were also assumed: (1) ω_{min} value of the Rayleigh damping function equal to the frequency of the sinusoidal input, and (2) quiet boundaries, under free-field conditions, to simulate a lateral infinite medium. Under these assumptions, no boundary reflection waves were generated within the 2-D model.

[33] When the 2 Hz sinusoidal inputs for all the assumed amplitudes were applied to this numerical model, the equilibrium was always obtained under both coseismic and postseismic conditions. The same result was obtained using a 1 Hz input with a 0.01 m/s^2 amplitude. Conversely, using a 1 Hz input with a 0.1 m/s^2 amplitude resulted into coseismic disequilibrium (Figure 8). In this instance, the slope failure mechanism was very similar to the actual one, as (1) the main rupture surfaces well fitted the geometry of the reconstructed landslide mass (see location of rupture surfaces at ground level and in boreholes S1 and S2), and (2) the displacement field exhibited a simultaneous translation of the landslide mass of some tens of decimeters. The simulated displacements were very consistent with those measured after the landslide reactivation [*Bozzano et al.*, 2004b]. Furthermore, the deformation of the clay shales involved in the landslide exceeded the volumetric dynamic threshold resulting from the shear modulus degradation curve. This finding was consistent with the large deformations appearing in the landslide mass after applying the dynamic input. A new static equilibrium was achieved under postseismic conditions and many yielding shear zones developed in the landslide mass.

[34] Since the 0.1 m/s^2 is an input amplitude value which significantly exceeds the acceleration value inferred at the Salcito site from the CMM record, local amplification effects may be invoked.

[35] A pseudostatic safety factor FS > 2 was calculated using the relation by *Newmark* [1965]:

$$FS = (t)[(\cos\beta - k_h(t)\sin\beta)\tan\phi]/(\sin\beta + k_h(t)\cos\beta) \quad (4)$$

where β is dip of the slope equal to 8°; ϕ is friction angle along the sliding surface equal to 22°; and k_h is yield coefficient equal to $a_{max}/g = 3.2 \times 10^{-3}$. The latter value was obtained for an equivalent PGA = 0.032 m/s^2 accounting for 65% of the PGA recorded at the CMM accelerometric station.

[36] A yield acceleration $a_y = 2.4$ m/s^2, to induce pseudostatic disequilibrium, was also computed using the relation by *Jibson* [1993]:

$$a_y = (FS - 1)\, g\, \sin\beta \quad (5)$$

by assuming an inclination (β) of 8° and a static safety factor for translational movement (FS) of 2.8.

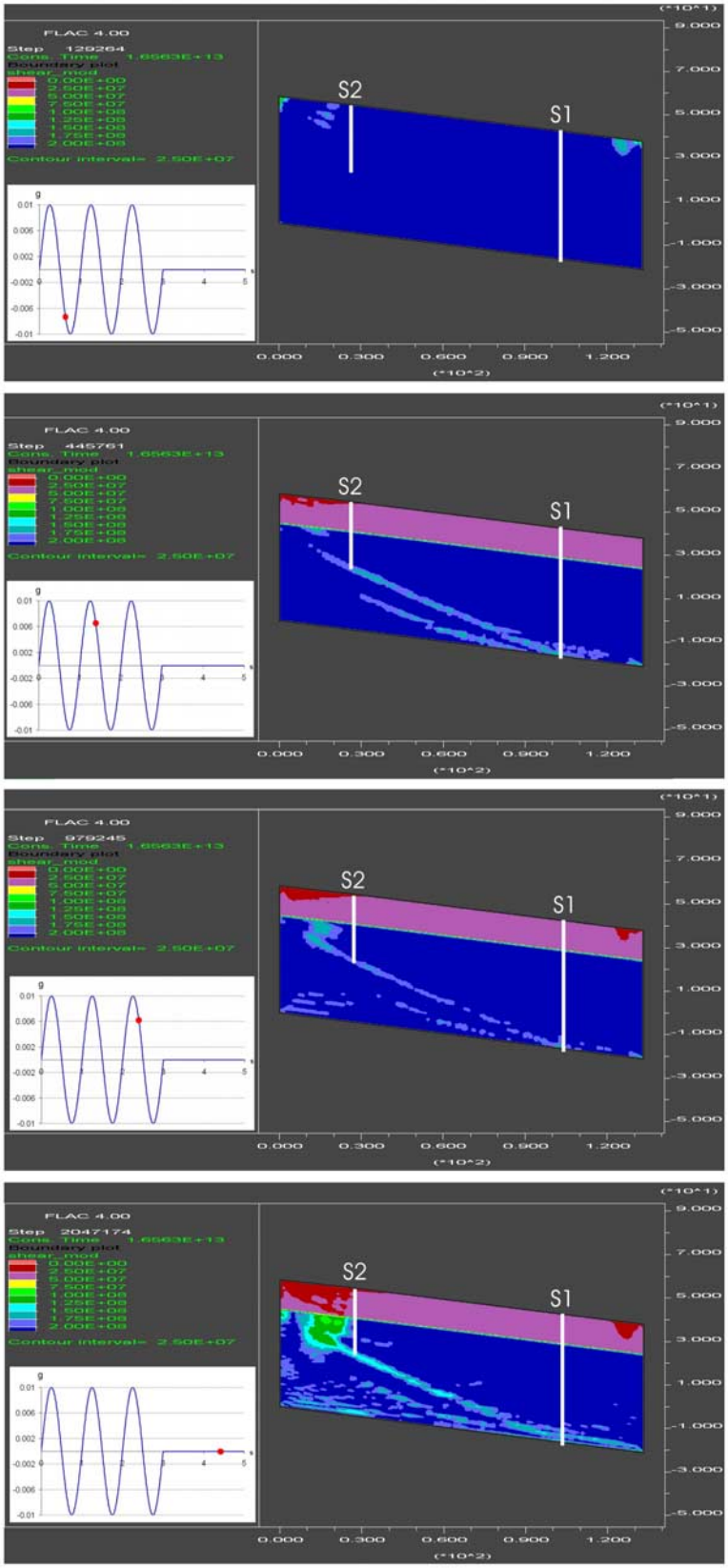

Figure 8. Dynamic numerical modeling (FLAC 5.0 software) of the Salcito landslide trigger, using a 1 Hz sinusoidal equivalent input with a duration of 5 s and an amplitude of 0.01 m/s^2: note (from top to bottom) a sequence of dynamic shear modulus (G) contours (up to 2.00×10^8 Pa with an interval of 2.50×10^7 Pa) at 0.6, 1.4, 2.4, and 4.4 s. The lowest values of the G modulus identify the zones of plastic flow along rupture surfaces. Note the location of the S2 and S1 boreholes (see also geological section in Figure 3).

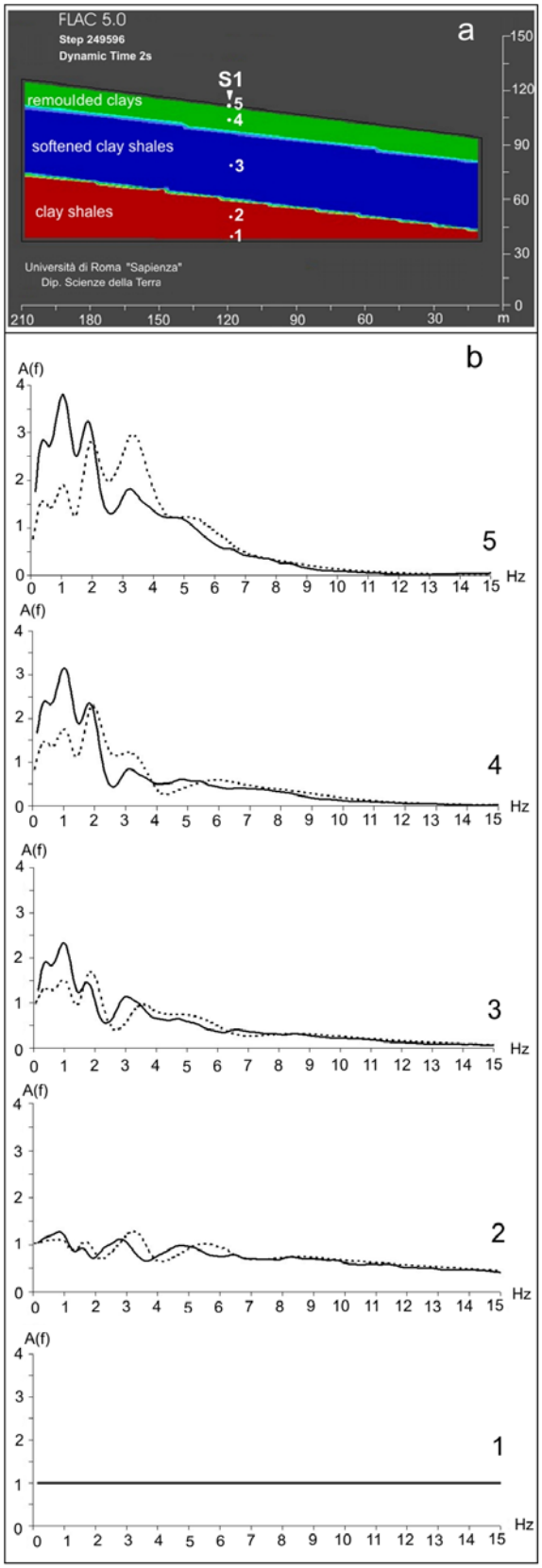

Figure 9. (a) Numerical infinite slope model of the Salcito landslide, used in the FLAC 2-D analysis of local seismic response; (b) transfer function (A(f)) obtained along the S1 vertical line with the FLAC 2-D numerical model under linear (dashed line) and nonlinear conditions (solid line).

[37] The values calculated for both the pseudostatic FS and the critical pseudostatic acceleration do not justify the observed seismic triggering of the Salcito landslide, unless local amplification effects are taken into account. However, the critical PGA value for landslide triggering obtained from pseudostatic analysis is about one order higher than the value obtained from dynamic analysis.

[38] The inclination of the lower boundary of the simulated model proved not to affect the kinematic solution of slope instability, but to significantly alter seismic wave propagation in the numerical model. Therefore, using FLAC 5.0, a 2-D numerical model with a horizontal lower boundary was built along the same engineering geology section, with a view to investigate the local seismic response due to the landslide mass [*Havenith et al.*, 2002, 2003a, 2003b; *Bourdeau*, 2005].

[39] A specific delta-like Gabor function ($G(t)$) was applied to the lower boundary. Output acceleration time histories were obtained along a vertical scan line running from the model bottom to the landslide surface. The analytical expression of $G(t)$ is

$$G(t) = e^{\left[\frac{2\pi f_p (t-t_S)}{\mu}\right]^2} \cos\left[2\pi f_p (t - t_s) + \varphi\right]. \quad (6)$$

where μ is coefficient related to the frequency range of the FFT, f_p is central frequency value of the FFT, t_s is value for time translation, and φ is phase parameter, equal to 0.066, 0.45, 0.066, and $\pi/2$, respectively. The choice of the latter parameters ensured a $G(t)$ FFT with nonnegligible spectral amplitudes up to frequencies of about 15 Hz. The Gabor function was defined to be energy equivalent to the main shock acceleration time history. Moreover, to avoid numerical errors during dynamic calculation, the function was assumed to have a symmetrical shape and a null integral.

[40] An amplification function A(f) was defined as the spectral ratio between the surface and bottom simulated acceleration time histories. Two-dimensional local seismic amplification analysis was conducted using FLAC 5.0 under both linear and nonlinear conditions: under nonlinear conditions, use was made of the same dynamic properties (i.e., G/G_0 and D/D_0 versus γ curves) as those applied in stability analysis (Figure 6). Results indicated an A(f) function with three frequency peaks, at about 1, 2, and 3 Hz, respectively. Nonlinear simulation yielded higher amplitude values for the resulting frequency peaks at 1 and 2 Hz, while the 3 Hz frequency peak was significantly reduced (Figures 9 and 10a). Comparing the transfer functions A(f) obtained along the S1 vertical line (Figure 9, points 1–5), both inside and below the landslide mass, suggests that all the frequency peaks are amplified only within the landslide mass. In nonlinear dynamic analysis, the highest frequency peak has lower values (Figure 9b).

6. Ambient Noise Records

[41] Starting from the results of the dynamic numerical modeling, local amplification of ground motion was assumed to favor the landslide event. A seismic survey was thus planned to assess this effect. Given the very low rate of seismic occurrence in the landslide area, a temporary array

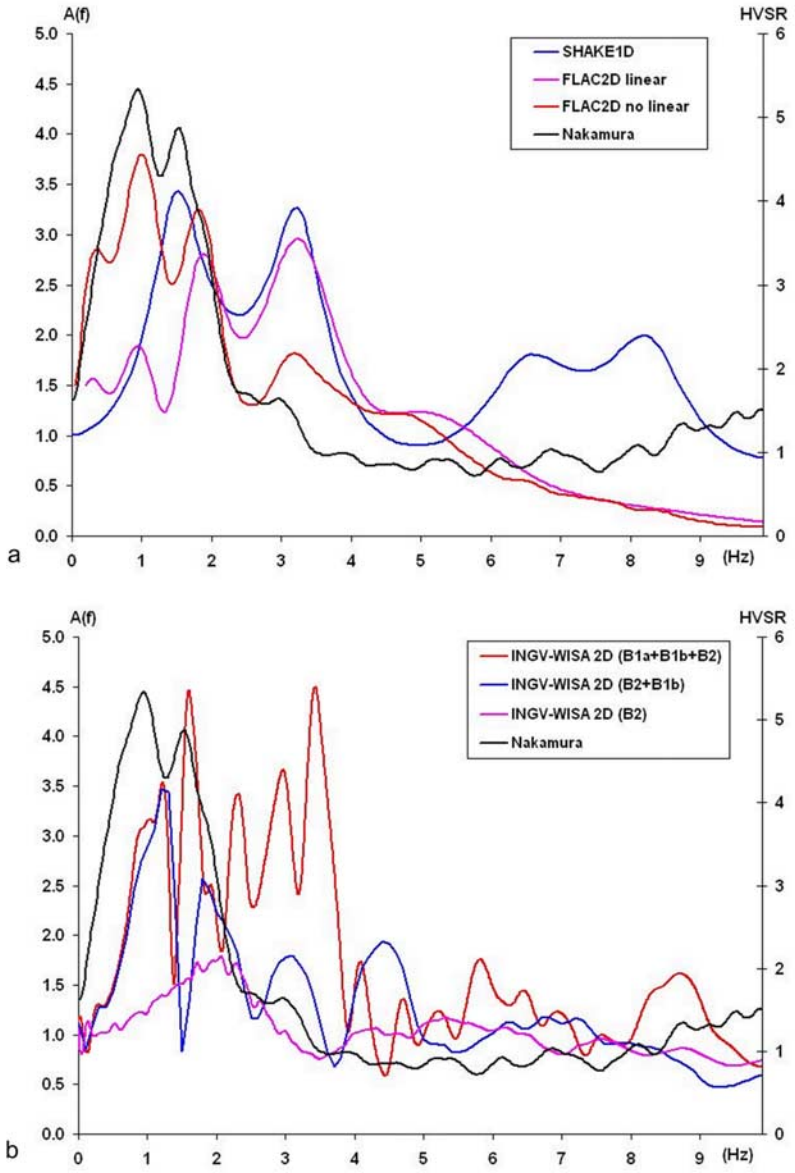

Figure 10. Comparison between the HVSRs obtained with the Nakamura technique and the transfer function (A(f)) obtained for receiver station 6 (S1 borehole within the landslide mass) with (a) the SHAKE and FLAC numerical models and (b) the INGV-WISA model.

would have not recorded a representative number of weak motions. Therefore, use was made of the *Nakamura* [1989] technique in lieu of the reference station methodology [*Borcherdt*, 1994].

[42] The geophysical survey was planned in two stages:

[43] 1. In the first stage, recording stations were distributed (about 300 m apart, stations 1 to 10, Figure 11) over the investigated slope based on geomorphological features; in particular, coupled stations were placed inside and outside the landslide mass, in the detachment area, in the toe area and along the flanks, while station 1 was positioned at a distance of about 1.5 km from the right side of the landslide on a flat rock site;

[44] 2. In the second stage, the distribution of recording stations (about 100 m apart, stations 11 to 24, Figure 11) was denser within the landslide area where significant amplification effects had been identified by previous measurements. This distribution was independent of geomorphological features and was only intended to permit the spatial analysis of the results.

[45] In each selected site, ambient noise was monitored for about 15 min by a moving station equipped with SS1 Kinemetrics triaxially arranged velocimeters (1 Hz) and a K2 Kinemetrics digital data logger.

[46] At least a second noise sample was taken overnight, if amplification effects were observed. The recorded ambient noise was sampled with a 40 s moving time window and FFT (Fast Fourier Transform) transformed to the frequency domain in order to get the average spectra of the three components (NS, UP, WE) for each station and each sampling. The H/V spectral ratios (HVSR) of the two horizontal components obtained in each station were com-

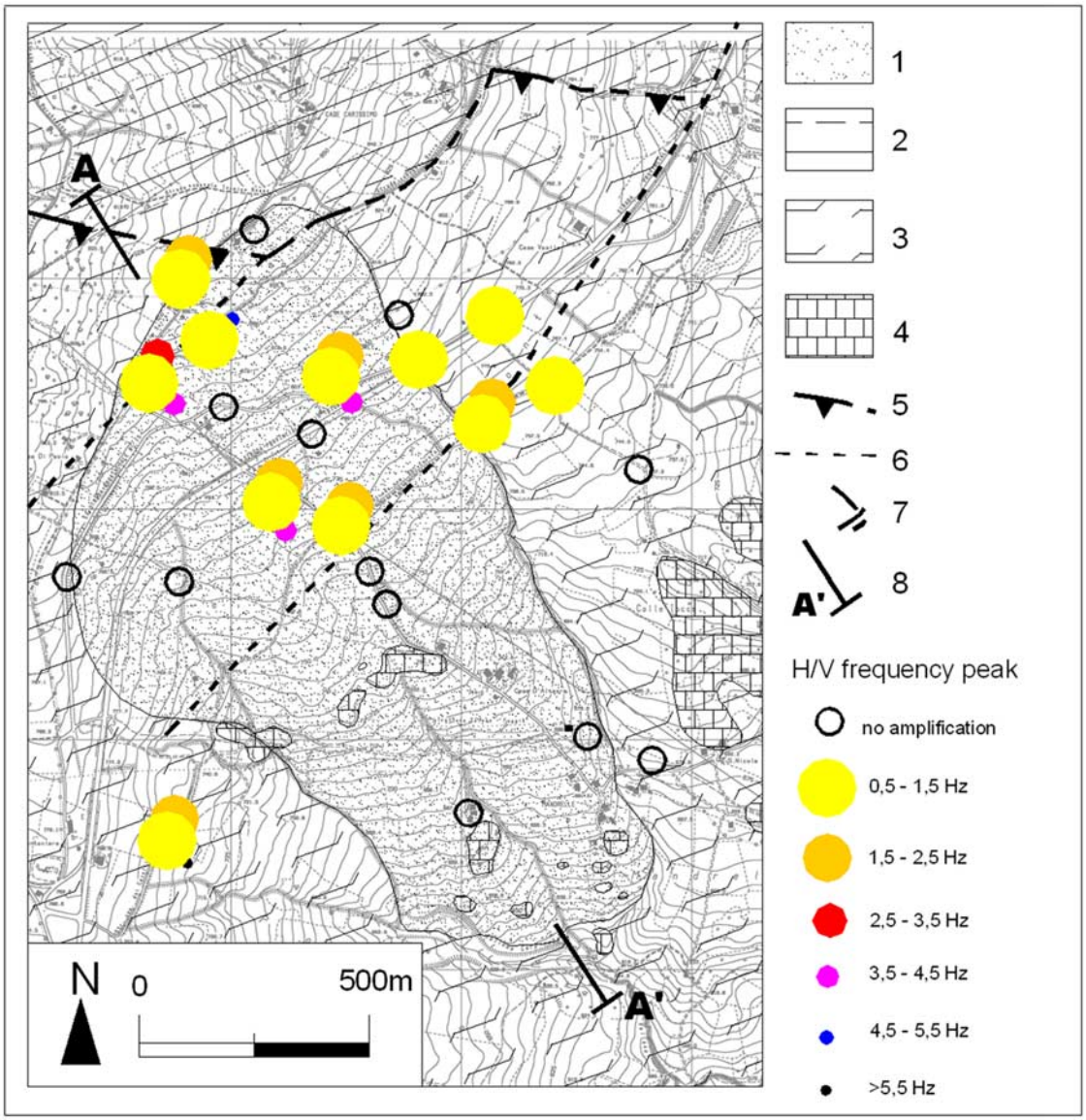

Figure 11. Amplification frequencies from HVSRs in the Salcito landslide area: 1, landslide mass; 2, marls with calcarenites of the Tufillo Formation; 3, fissured clay shales of the Argille Varicolori Formation; 4, calcarenites and marls of the Sannio Unit; 5, thrust; 6, tear fault; 7, ground crack observed after the Salcito landslide reactivation of 31 October 2002; 8, trace of geological section.

pared. As no systematic directional effect was identified, use was made of the average HVSR. Only HVSR values greater than 2 were considered, in accordance with the SESAME (Guidelines for the implementation of the H/V spectral ratio technique on ambient vibrations, 2004, http://sesame-fp5.obs.ujf-grenoble.fr/index.htm) standards. Significant values were clustered into six frequency classes in the 0.5–6.5 Hz range. Results are plotted in Figure 11 for each recording station; stations with no amplification are also shown. HVSR values point out an amplification zone upslope, near the left flank of the landslide. The main HVSR peaks correspond to frequency values in the 1–2 Hz range, whereas frequency values in the 3.5–4.5 Hz range are only observed within the landslide mass. Further peaks in the 5.5–6.5 Hz frequency range are noted within the landslide mass, very close to the main scarp. No amplification effects are visible in the right portion of the slope. All of the HVSR show an asymmetrical distribution of frequency peak values within the landslide mass.

7. One- and Two-Dimensional Numerical Modeling of Local Seismic Response

[47] Local seismic response was analyzed under two different approaches, based on 1-D and 2-D simulations, respectively. The analysis aimed at evaluating the role of local seismic conditions in amplifying and altering the input motion. One-dimensional simulations were conducted in the frequency domain by means of a software based on the Thomson-Haskell method [*Haskell*, 1962]. Two-dimensional simulations were made in the time domain by using a finite difference method (FDM) and following the general-

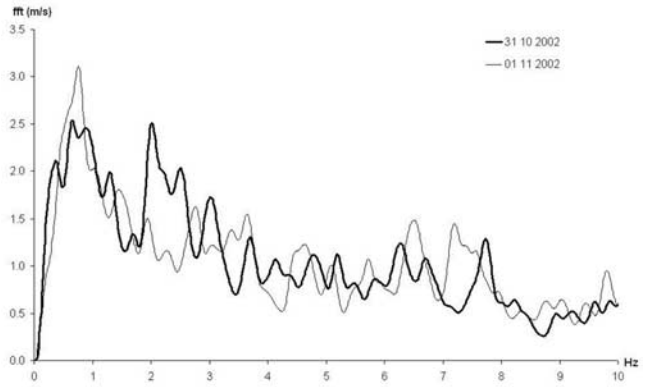

Figure 12. Fourier spectra of the Molise earthquake main shocks recorded at the Castiglione Messermarino (CMM) accelerometric station (see Figure 1 for location).

ized Maxwell body idea [*Emmerich and Korn*, 1987]. In particular, the synthetics of 2-D modeling were obtained by using the WISA software developed by Istituto Nazionale di Geofisica e Vulcanologia (INGV) to study dynamic interaction between seismic radiation and near-surface geological structures [*Caserta et al.*, 2002]. In the frequency domain, both linear and nonlinear modeling was performed; in the latter, influence of nonlinearities during propagation was simulated using the iterative procedure of the equivalent linear model available in the SHAKE software [*Schnabel et al.*, 1972].

[48] In all of the 1-D simulations, an infinite geometry, composed of three strata parallel to the slope, was assumed for geotechnical zoning (Figure 7d). The first 15 m layer was associated with soil composed of clay shales and the second underlying 35 m layer with medium-consistency clay shales in the landslide body. For both layers, a viscoelastic rheology was assumed. Stiffness and damping decay versus shear strain curves were obtained from dynamic cyclic laboratory tests. In particular, in linear modeling, shear stiffness and damping values obtained from laboratory tests at the lowest strain levels have been used. Conversely, in nonlinear modeling, the shear stiffness and the damping decay curves have been taken into account (Table 1 and Figure 6). The third layer, corresponding to the substratum, was assumed to be elastic and has a shear wave velocity of 990 m/s. In the linear 1-D simulation, no input was used to reconstruct the seismic transfer function, i.e., the ratio of the FFT amplitudes calculated at the top of the soil column to those at the outcropping bedrock. In nonlinear simulation, the transfer function depends on the input data; thus, the main shock recorded at the CMM on 31 October was taken as input at the outcropping bedrock (Figure 12). However, the maximum acceleration value corresponding to the CMM record was insufficient to induce a nonlinear behavior in 1-D simulation. As a consequence, no significant difference emerged between linear and nonlinear 1-D simulations. By contrast, the transfer function A(f), derived from FLAC 5.0 2-D dynamic modeling, turned out to be significantly different depending on whether linear or nonlinear conditions were considered (see paragraph 5). In particular, the transfer function A(f) obtained under nonlinear conditions is very similar to the HVSR derived from noise records (Figure 10a). The transfer function calculated with a frequency resolution of 0.1 Hz is shown in Figure 10a. The greatest amplification is found in a 1–4 Hz double-peak frequency band. The first peak (about 1.8 Hz, amplification value of 3.5) is related to the total thickness of the landslide mass and to the average velocity of the two layers. The second peak (about 3 Hz, amplitude of 3.2) is related to the internal layering of the landslide mass and, in particular, to the thickness of the upper layer and its velocity. A further 6–9 Hz frequency band has amplitudes not exceeding 2.

[49] In order to perform 2-D numerical simulations, the engineering geology model of Figure 7a was transposed into a basin-like physical model (Figure 7b). This model consists of two basins: a shallow basin representing the landslide mass (B1) and a larger and deeper basin with Argille Varicolori embedded in a marly and calcarenitic bedrock, representing the local geological setting (B2). Moreover, the B1 basin holds two layers, which correspond to the 15 m thick layer of superficial remolded clays (B1a) and to the clay shales of the landslide mass, down to 50 m bgl (B1b), respectively.

[50] Three linear 2-D simulations with the INGV-WISA software were run in order to separately analyze the role of the two basins in the physical model. The corresponding domains of integration were digitized using the WISA tool, based on a Web user-friendly interface [*Santoni et al.*, 2004]. For all the simulations, the numerical model was divided into a 392 $\times$ 799 grid representing a 500 m deep and 7080 m long rectangular domain. The constant spatial step Δl was set to 0.5 m and the temporal one to Δt 2.45 $\times$ 10^{-4} s. The corresponding maximum admissible frequency of the model, f = $V_s/10\Delta$l [*Kuhlemeyer and Lysmer*, 1973], always lies well above 10 Hz. Within the stratigraphy at 230 m bgl, the input was given in the form of a vertical upward SH antiplanar wave, represented by the previously defined Gabor function *G(t)* in its asymmetrical shape. Damping of the soils was represented by a "nearly constant Q" linear viscoelastic model [*Liu et al.*, 1976].

[51] One 2-D simulation (I) was run (Figure 13) considering only the basin with the embedded Argille Varicolori (B2), with dimensions of about 1 km and 140 m (Figure 13b). The shear wave velocity was set to 990 m/s and the quality factor to 10, as suggested by the values recorded by the authors at the bottom of a landslide mass in a similar formation of fissured clay shales [*Bozzano et al.*, 2008].

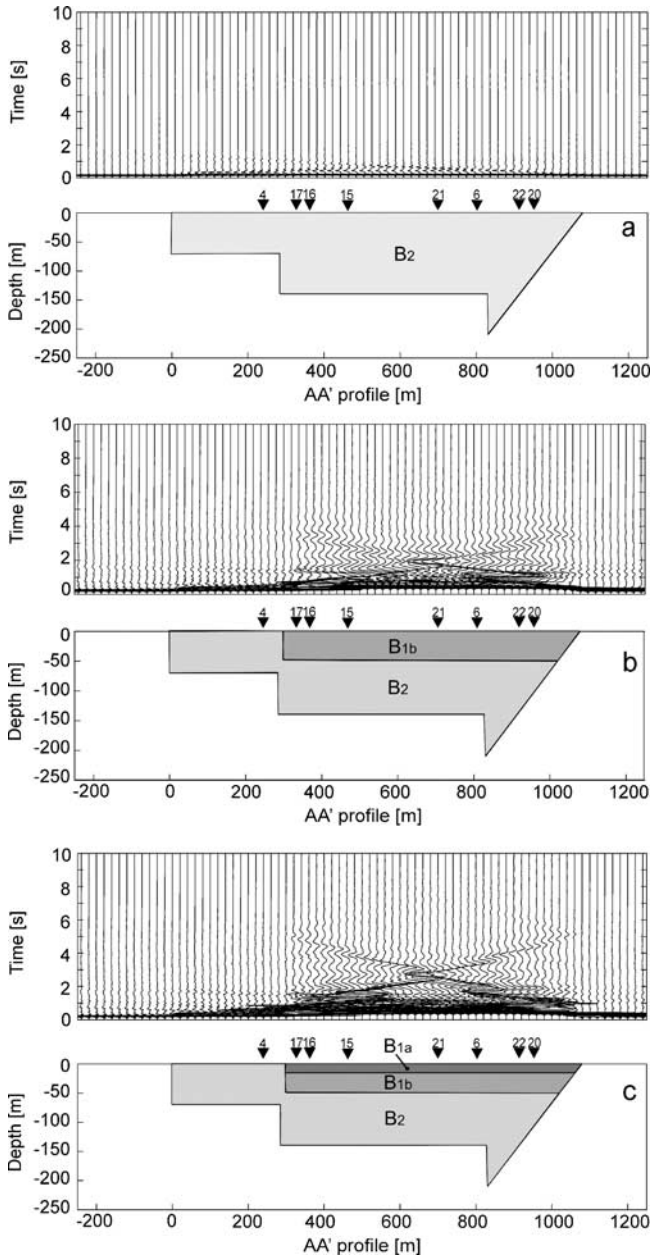

Figure 13. Seismic wave propagation in the INGV-WISA model for the three simulated basin-like conditions: (a) only B2 basin; (b) B2 + B1b basins, (c) B2 + B1b + B1a basins.

For the underlying half-space, a shear wave velocity of about 1450 m/s and a Q value of 50 were assumed. The two other simulations (II and III) also took into consideration the landslide basin (B1). In simulation II, the B1 basin was modeled by a single 50 m layer composed of clays shales; in simulation III, the same B1 basin was simulated by the two layers (B1a and B1b) used in the 1-D linear simulation. The landslide basin (B1) was always boxed in the geological basin (B2) and the same half-space was considered. The spectral outputs obtained from the displacement time histories were filtered with a low-pass filter (<15 Hz).

[52] The wave propagations obtained along the entire horizontal profile at the top of the stratigraphies are shown in Figure 13, in the AA' portion of the investigated domain. The maximum dimensions of the largest basin were however smaller than those of the overall simulated domain; this choice was made to avoid effects associated with nonphysical numerical lateral reflections in the synthetic outputs. The generation of Love surface waves was concentrated at the edges of the basins in all the simulations. The models with the landslide mass (B1), in particular simulation III, proved to alter the input motion much more significantly, since the synthetics had a longer duration and a higher amplitude (Figures 13b, 13c).

[53] For all the simulations, the outputs obtained at the model surface along the entire horizontal domain were FFT transformed (Figure 14). The outcropping reference station was placed halfway between the left boundary of the model and the left edge of the B2 basin. The spectral ratios to the reference point were obtained for the synthetic displace-

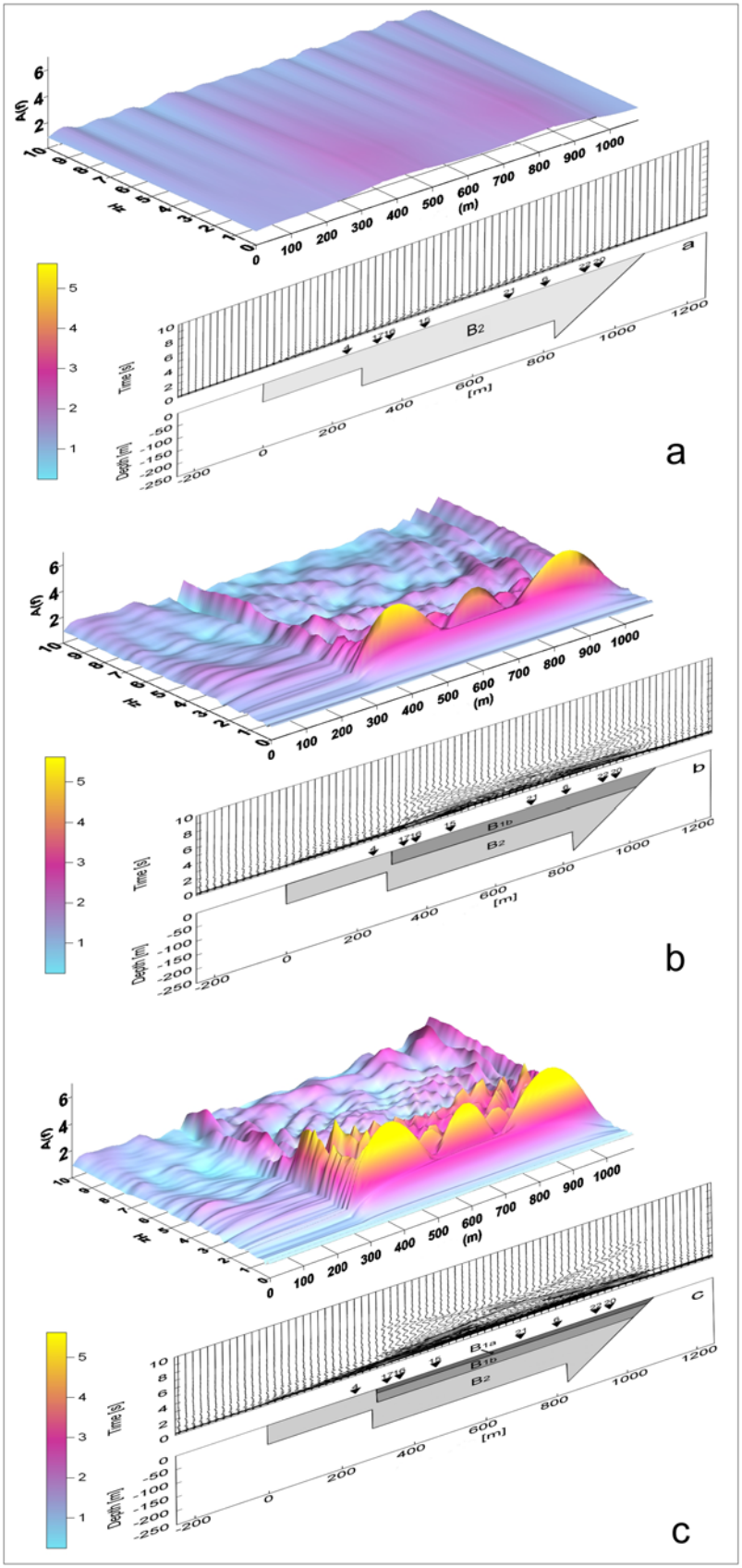

Figure 14. Transfer functions (A(f)) obtained along the INGV-WISA basin-like model in the 1–10 Hz frequency range and related wave propagation under the three simulated basin-like conditions: (a) only B2 basin; (b) B2 + B1b basins, (c) B2 + B1b + B1a basins.

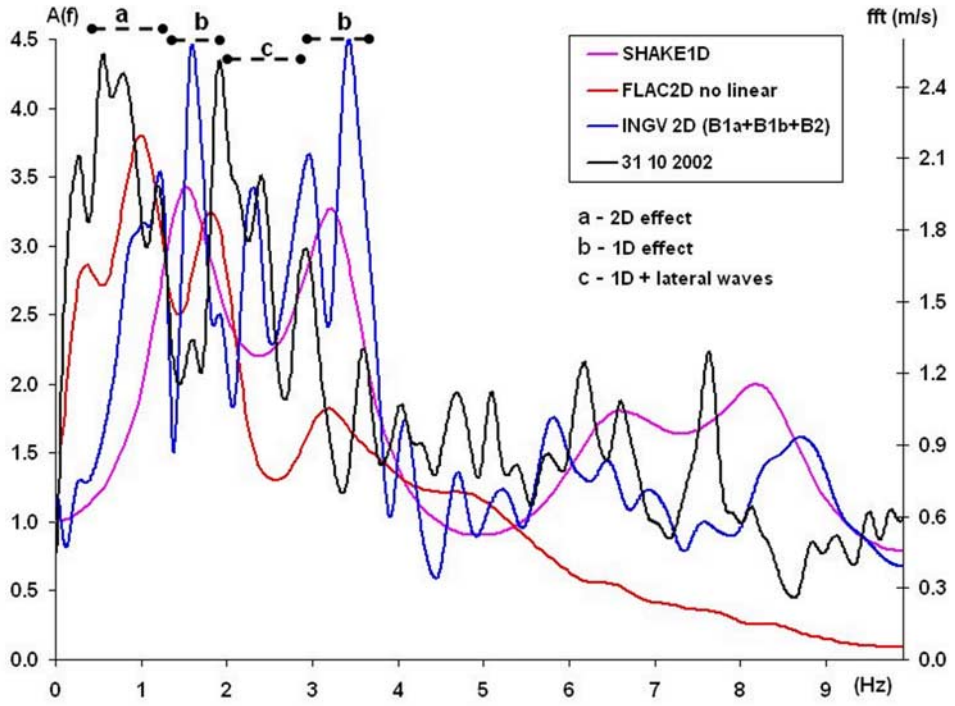

Figure 15. Transfer functions (A(f)) simulated with SHAKE1D, FLAC and INGV-WISA compared with the Fourier spectrum of the main shock (31 October 2002) recorded at the CMM accelerometric station and responsible for triggering the Salcito landslide.

ments all along the AA' section. The spectral ratios from simulation I indicated that the B2 basin did not significantly contribute to amplifying the input motion (Figure 14a); on the contrary, simulations II and III demonstrated the crucial role of the landslide mass in inducing amplification effects (Figures 14b, 14c, and 15).

[54] Although the landslide profile has an asymmetrical form, its maximum depth (50 m) and half width (390 m) can be used to determine its shape ratio. The resulting value of 0.13, permitted to classify the landslide system like a shallow sediment-filled valley [*Bard*, 1983; *Bard and Bouchon*, 1985; *Bard*, 1995] in both simulations II and III. The velocity contrast between the landslide mass and the surrounding soils was fixed between 3 and 3.5, as confirmed by the A(f) function from 1-D simulations (Figure 10a). The values of shape ratio and velocity contrast suggest that propagation in the landslide mass is affected by 1-D plus lateral wave effects [*Bard and Bouchon*, 1985]. As a consequence, in simulations II and III, A(f) has a more complex configuration and a greater number of narrow and adjacent frequency peaks, with amplification values higher than those obtained from 1-D simulations. In particular, the amplitude values obtained in simulation III (B1b and B1a) are up to 2 times higher.

[55] Figures 14 and 16 show A(f) along the horizontal section delimited by the left and the right edges of the B2 basin. Simulation II (Figures 14b and 16b) shows lower amplitudes of A(f) than simulation III (Figure 14c and 16c) throughout the frequency range. In simulations II and III, the most important difference in amplitude values is observed in the 2–4 Hz frequency range. In simulation II, the maximum A(f) amplitude is about 5 (at 1.7 Hz) and, for higher frequencies (>2 Hz), amplitude values are always below 2.5. Simulation III gives a first frequency band, in the 0.5–1.5 Hz range, containing the maximum A(f) value (about 7). The absence of this resonance frequency in the 1-D transfer functions suggests that it is closely related to the 2-D nature of the basin-like system. In both simulations II and III, the maximum A(f) values lies close to the lateral boundaries of the landslide, while a relative maximum is found in the middle portion of the basin. Simulation III yields a second frequency band, in the 1.5–2 Hz range, including the first 1-D resonance frequency at about 1.8 Hz, with an A(f) value of 3.5. The same simulation gives a third frequency band, in the 2.5–3.5 Hz range, in which the second mode of the 1-D transfer function of the landslide mass is identified (amplification value of about 3). Finally, for frequencies above 3.5 Hz, the A(f) amplitudes decrease to values lower than 2.

8. Final Remarks

[56] A multidisciplinary experimental approach was tested to analyze the mechanism of seismic activation of a large earth slide.

[57] Seismometric data as well as 1-D and 2-D numerical modeling were used to define the contributions of the different geological elements to local seismic response. A complex physical basin-like model was derived from engineering geology and geophysical investigations. In the model, the Salcito landslide mass corresponds to a shallow basin, placed in two different layers resulting from soil softening, weathering and alteration; a deeper basin is defined by the geological bedrock.

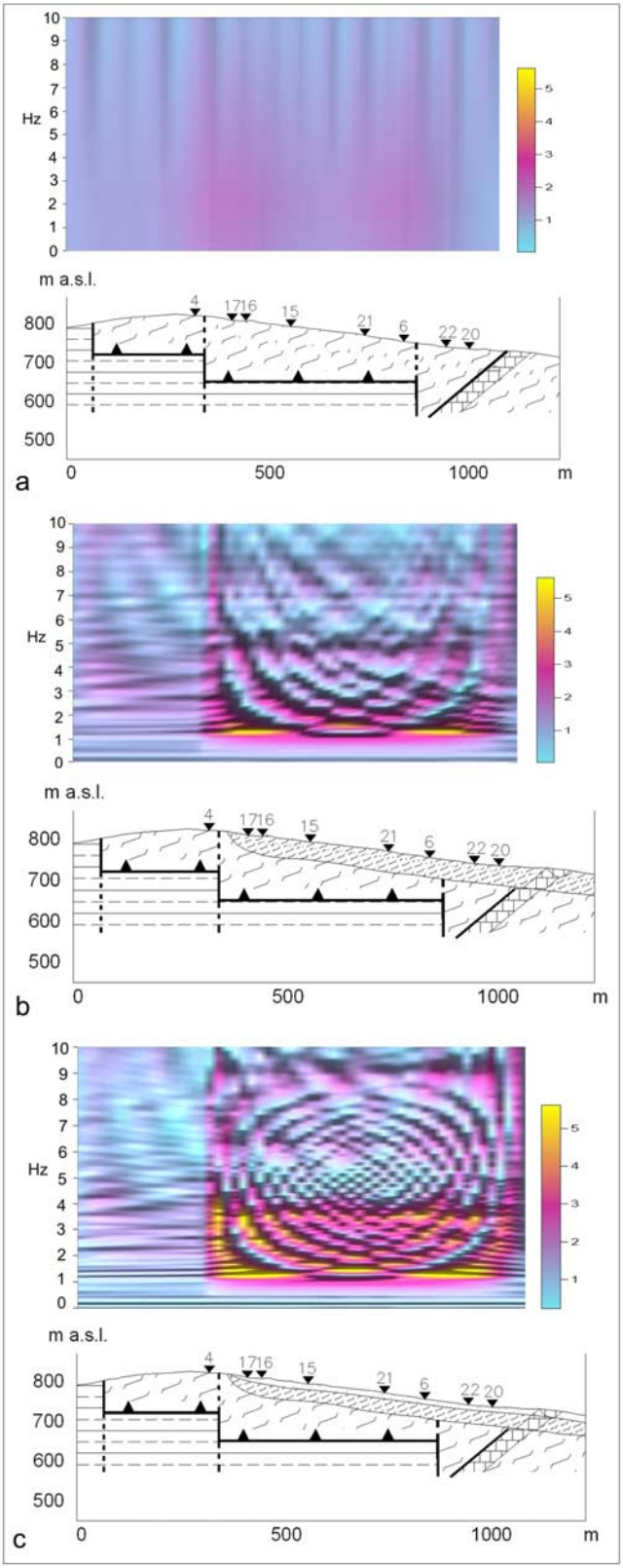

Figure 16. Transfer functions (A(f)) obtained along the INGV-WISA basin-like model in the 1–10 Hz frequency range, transposed into the evolution of the slope involved in the Salcito landslide: (a) prefailure slope; (b) slope after the first landslide activation; (c) actual slope.

[58] The interaction between the Salcito landslide mass and seismic waves, propagating from 300 m bgl, was investigated to evaluate the role of local seismic amplification in reactivation of the existing landslide. Different approaches were used to analyze local seismic response of the landslide mass; a 1-D elastic numerical modeling (Haskell-Thomson approach) was employed to obtain the transfer function of the vertical soil column, referred to the landslide mass stratigraphy,

[59] A 1-D linear-equivalent modeling (SHAKE1D software) was performed to get the amplification function (A(f)) of the vertical soil column, referred to the landslide mass stratigraphy and a 2-D linear and nonlinear dynamic model by FLAC 5.0 software was implemented to compute amplification functions (A(f)) referred to the landslide mass, taking into account the G/G_0 and D/D_0 versus γ decay curves through a time marching solution.

[60] Moreover, 2-D linear models by the INGV-WISA software were performed to obtain both wave propagation modes and amplification functions (A(f)) referred to a large-scale geological model, taking into account the local structural setting and the landslide mass via a two-layer model. These latter models can be considered to be significant for an about 500 m wide portion of the slope astride the AA' geological section of Figure 3.

[61] The comparison between ambient noise records, processed with the Nakamura technique, and numerical modeling results made it possible to distinguish contributions to the local seismic response attributable to 1-D as well as 2-D effects. The response is given by the combined effect of the landslide mass and of the local structural setting: the landslide mass, the deposits of clay shales and the underlying tectonized marly calcarenites define a double basin-like system. This system is composed of a small shallow basin (B1), filled with the Salcito landslide mass, and of a deeper basin (B2), filled with clay shales and bounded by the tectonized marly calcarenite bedrock. Moreover, within the B1 basin, two layers may be distinguished: a first layer (B1a) of remolded and softened clays (down to 15 m bgl) and a second layer (B1b) of medium- to high-consistency and structured clay shales (down to 50 m bgl). The resulting amplification effects are mainly due to the shallow basin-like structure, corresponding to the Salcito landslide mass. No significant amplification effect is observed if the B2 basin alone is modeled with the 2-D INGV-WISA software.

[62] A frequency peak at about 1 Hz in the A(f) function is obtained with both the FLAC and INGV-WISA 2-D modeling approaches, as well as with HVSR (Figure 15). In particular, the spatial distribution of A(f) at 1 Hz, obtained with the INGV-WISA model along a transversal section across the B1 basin, shows three peaks. These peaks may be related to the B1 boundaries, as well as to the interference waves acting in the middle portion of the basin (Figures 14b and 14c). The same 1 Hz frequency peak, obtained with the FLAC 2-D model, may be regarded as an effect of downslope dipping of the B1a and B1b layers within the landslide mass. Therefore, the 1 Hz frequency is amplified by two different 2-D effects and cannot be related to 1-D resonance, as demonstrated by the Haskell-Thomson and SHAKE 1-D models. Nevertheless this point is also evidenced by the Nakamura spectral ratios.

[63] A frequency peak at about 1.8 Hz results from both 1-D and 2-D numerical modeling as well as from the Nakamura spectral ratios. This frequency peak may be ascribed to a 1-D effect, which is closely related to the deposits (B1a and B1b) filling the B1 basin (Figure 16). A frequency peak at about 3 Hz also results from both 1-D and 2-D numerical modeling. This peak can be referred to the B1a layer lying within the landslide mass and causing a double-layer effect [*Meric et al.*, 2005] due to internal layering of the landslide mass. Hence, the above mentioned 1.8 and 3 Hz peaks may be regarded as the first two modes of the 1-D transfer function of the landslide mass (Figure 16). Additional frequency peaks ranging from 2.5 to 3.5 Hz are observed only in the INGV-WISA 2-D numerical model. As these peaks are clustered near the B1 lateral boundaries (Figure 16), they may be attributed to a 1-D plus lateral wave effect due to wave propagation within the B1 basin. Frequency peaks below 1 Hz, only obtained in 2-D models, are regarded as numerical effects due to the degrees of freedom of all the models and related to nonreflecting quiet boundaries.

[64] The comparison of the different modeling approaches with seismometric data confirms the critical role that the Salcito landslide mass played in the reactivation event, as can be inferred from the following findings: (1) an input with a main frequency content of about 1 Hz can reactivate the landslide, if a threshold energy level is reached; (2) the landslide mass (B1 basin) is responsible for amplification of ground motion in the 1–3 Hz range, due to 1-D and 2-D effects (Figure 16); and (3) the Fourier spectrum of the 31 October 2002 main shock has two main frequency peaks at 1 and 2 Hz, respectively (Figure 12).

[65] Since the earthquake-induced frequencies were amplified by the landslide mass and are consistent with its sliding mechanism, the Salcito landslide reactivation may be regarded as a seismically induced self-excitation phenomenon. The three different conditions simulated with the INGV-WISA 2-D numerical software may be referred to the following evolutionary steps of the Salcito landslide slope (Figure 16): (1) No landslide is present on the slope (only B2 basin); (2) A first-activation landslide mass is present on the slope, not necessarily consequent upon seismic triggering (B_{1b}+B_2); and (3) A next-activation landslide is present on the slope; the slope has a softened superficial stratum resulting from minor landslides, which were induced by seasonal rainfall or creep processes (B_{1a} + B_{1b} + B_2).

[66] In particular, the INGV-WISA model demonstrates that the B1a layer plays a major role in inducing seismic amplification at frequencies of 2.5–3.5 Hz. Moreover, nonlinear effects in terms of A(f) values (Figure 10a) prove to be significant in landslide triggering, in that they increase the stiffness contrast between the landslide mass (strongly involved in stiffness decay) and the substratum. In contrast, the superficial layers of softened soil within the landslide mass, due to Earth flow processes as well as to weathering and alteration of the clay shales, produce a double-layer soil column. The latter is responsible for a second resonance mode (3 Hz) which reduces the A(f) value of the first one (2 Hz). The results achieved in the study give new insights into seismically induced effects driven by self-excitation processes on large existing landslides. Indeed, landslide masses may generate significant amplification effects at low frequencies (of up to 2 Hz), consistent with their sliding mechanisms.

[67] The study also indicated that, after the first activation, a landslide becomes prone to seismically induced reactivations, owing to local amplification of the landslide mass itself at low frequencies (of up to 2 Hz), and the superficial softening of the landslide mass, due to minor and seasonal landslides, favors lateral wave interactions, thereby enhancing seismic amplification at higher frequencies.

[68] **Acknowledgments.** The authors are indebted to D. Jongmans and A. Rovelli for their helpful suggestions and oral communications; P. De Pari, M. R. Manuel, R. D'Elia, and M. Carelli for their contribution to field investigations. The authors also thank W. Z. Savage and an anonymous referee for their revision of the paper. Thanks also to the National Institute of Geophysic and Vulcanology (INGV) for permitting the use of the INGV-WISA code. This research study was funded as part of the PRIN2005 project "Induced seismic hazard: analysis, modelling, and predictive scenarios of earthquake triggered landslides" (Project Leader, G. Scarascia Mugnozza).

References

Ambraseys, N., and M. Srbulov (1995), Earthquake induced displacements of slopes, *Soil. Dyn. Earthquake Eng.*, *14*, 59–71, doi:10.1016/0267-7261(94)00020-H.

Bard, P. Y. (1983), Les effets de site d'origine structurale en sismologie. Modélisation et interprétation. Application au risque sismique, thèse d'Etat, Univ. Sci. et Méd. de Grenoble, Grenoble, France.

Bard, P. Y. (1995), Effects of surface geology on ground motion: Recent results and remaining issues, in *Earthquake Engineering: Proceedings of the* 10th *European Conference, Vienna, Austria, 28 August–2 September 1994*, edited by G. Duma, pp. 305–323, A. A. Balkema, Rotterdam, Netherlands.

Bard, P. Y., and M. Bouchon (1985), The two-dimensional resonance of sediment-filled valleys, *Bull. Seismol. Soc. Am.*, *75*, 519–541.

Bardet, J. P., and R. B. Seed (2000), Soil liquefaction, landslides, and subsidences, *Earthquake Spectra*, *16*, 141–162.

Bianchi Fasani, G., F. Bozzano, C. Esposito, M. R. Manuel, S. Martino, A. Prestininzi, and G. Scarascia Mugnozza (2004), An example of earthquake triggered landslide in structurally complex formations, in *Proceedings of IX International Symposium on Landslides (Rio de Janeiro)*, pp. 321–327 A. A. Balkema, Rotterdam, Netherlands.

Bird, J. F., and J. J. Bommer (2004), Earthquake losses due to ground failure, *Eng. Geol. Amsterdam*, *75*, 147–179, doi:10.1016/j.enggeo.2004.05.006.

Bonci, L., F. Bozzano, S. Calcaterra, V. Eulilli, F. Ferri, P. Gambino, M. R. Manuel, S. Martino, and G. Scarascia Mugnozza (2004), Geological control on large seismically induced landslides: The case of Cerda (southern Italy), in *Proceedings of IX ISL (Rio De Janeiro)*, pp. 985–991, A. A. Balkema, Rotterdam, Netherlands.

Borcherdt, R. D. (1970), Effects of local geology on ground motion near San Francisco Bay, *Bull. Seismol. Soc. Am.*, *60*, 29–61.

Borcherdt, R. D. (1994), Estimates of site-dependent response spectra for design (methodology and justification), *Earthquake Spectra*, *10*, 617–653, doi:10.1193/1.1585791.

Bordoni, P., and the Cavola Experiment Team (2005), Cavola experiment: A dense broadband seismic array on an active landslide, *Geophys. Res. Abstr.*, *7*, 07,7262005.

Bourdeau, C. (2005), Effets de sites et mouvement de versants en zones sismiques: Apport de la modélisation numérique, Ph.D. thesis, Ecole des Mines, Paris.

Bozzano, F., P. Gambino, I. La Rosa, and G. Scarascia Mugnozza (2001), Analisi preliminare degli effetti di superficie indotti dalla sequenza sismica Umbro-Marchigiana nei mesi di Settembre-Ottobre 1997, *Mem. Soc. Geol. Ital.*, *56*, 283–290.

Bozzano, F., E. Cardarelli, M. Cercato, M. R. Manuel, S. Martino, and G. Scarascia Mugnozza (2004a), Determinazione delle proprietà dinamiche delle formazioni coinvolte nella frana di Salcito (CB) del 31 Ottobre 2002 tramite prove geofisiche in sito e prove di laboratorio, paper presented at 23rd Convegno Nazionale del Gruppo Nazionale di Geofisica della Terra Solida, Rome.

Bozzano, F., S. Martino, G. Naso, A. Prestininzi, R. W. Romeo, and G. Scarascia Mugnozza (2004b), The large Salcito landslide triggered by the 31st October 2002, Molise earthquake, *Earthquake Spectra*, *20*(2), 1–11.

Bozzano, F., S. Martino, and M. Priori (2006), Natural and man-induced stress evolution of slopes: The Monte Mario hill in Rome, *Environ. Geol.*, *50*, 505–524, doi:10.1007/s00254-006-0228-y.

Bozzano, F., E. Cardarelli, M. Cercato, L. Lenti, S. Martino, A. Paciello, and G. Scarascia Mugnozza (2008), Engineering-geology model of the seismically-induced Cerda landslide, *Boll. Geofis. Teorica Appl.*, *49*(2), 205–226.

Cara, F., A. Rovelli, G. Di Giulio, F. Marra, T. Braun, G. Cultrera, R. Azzara, and E. Boschi (2005), The role of site effects on the intensity anomaly of San Giuliano di Puglia inferred from aftershocks of the Molise, central southern Italy, sequence, November 2002, *Bull. Seismol. Soc. Am.*, *95*(4), 1457–1468, doi:10.1785/0120040031.

Caserta, A., V. Ruggiero, and P. Lanucara (2002), Numerical modelling of dynamical interaction between seismic radiation and near surface geological structures: A parallel approach, *Comput. Geosci.*, *28*(9), 1069–1077, doi:10.1016/S0098-3004(02)00024-9.

Castello, B., G. Selvaggi, C. Chiarabba, and A. Amato (2005), CSI Catalogo della Sismicità Italiana 1981–2002, versione 1.0, Ist. Naz. di Geofis. e Vulcanol. *Centro Naz. Terremoti*, Rome. (Available at http://www.ingv.it/CSI/)

Cetin, K. O., N. Isik, and B. Unutmaz (2004), Seismically induced landslide at Degirmendere Nose, Izmit Bay during Kokaeli (Izmit)-Turkey earthquake, *Soil Dyn. Earthquake Eng.*, *24*, 189–197, doi:10.1016/j.soildyn.2003.11.007.

Chavez-Garcia, F. J., L. R. Sanchez, and D. Hatzfeld (1996), Topographic site effects and HVSR. A comparison between observation and theory, *Bull. Seismol. Soc. Am.*, *86*, 1559–1573.

Chavez-Garcia, F. J., M. Rodriguez, E. H. Field, and D. Hatzfeld (1997), Topographic site effects. A comparison of two nonreference methods, *Bull. Seismol. Soc. Am.*, *87*, 1667–1673.

Dai, F. C., C. F. Lee, J. H. Deng, and L. G. Tham (2005), The 1786 earthquake-triggered landslide dam and subsequent dam-break flood on the Dadu River, southwestern China, *Geomorphology*, *65*, 205–221, doi:10.1016/j.geomorph.2004.08.011.

Del Gaudio, V., and J. Wasowski (2004), Time probabilistic evaluation of seismically-induced landslide hazard in Irpinia (southern Italy), *Soil. Dyn. Earthquake Eng.*, *24*, 915–928, doi:10.1016/j.soildyn.2004.06.019.

D'Elia, B. (1983), La stabilità dei pendii naturali in condizioni sismiche, paper presented at XV Convegno Nazionale di Geotecnica, Assoc. Geotecn. Ital., Spoleto, Italy.

D'Elia, B., G. Federico, T. Pescatore, and F. Rippa (1986), Occurrence and development of large landslide (Andretta, Italy) reactivated by the November 23rd 1980 earthquake, *Geol, Appl. Idrogeol.*, *XXI*(II), 365–381.

Dipartimento della Protezione Civile (2004), The strong motion records of Molise sequence (October 2002–December 2003) [CD-ROM], Ufficio Serv. Sismico Naz., Serv. Sistemi di Monitoraggio, Rome.

Emmerich, H., and M. Korn (1987), Incorporation of attenuation into time-domain computations of seismic wave fields, *Geophysics*, *52*(9), 1252–1264, doi:10.1190/1.1442386.

Esposito, E., G. Luongo, A. Maturano, and S. Porfido (1987), Il terremoto di S. Anna del 26 luglio 1805, *Mem. Soc. Geol. Ital.*, *37*, 171–191.

Evans, S. G., and A. L. Bent (2004), The Las Colinas landslide, Santa Tecla: A highly destructive flowslide triggered by the January 13, 2001, El Salvador earthquake, in *Natural Hazards in El Salvador*, edited by W. I. Rose et al., *Spec. Pap. Geol. Soc. Am.*, *375*, 25–37.

Faccioli, E. (1995), Induced hazard: earthquake triggered landslides, paper presented at the Fifth International Conference on Seismic Zonation, Earthquake Eng. Res. Inst., Nice, France.

Field, E. H., and K. Jacob (1995), A comparison and test of various site response estimation techniques, including three that are non reference-site dependent, *Bull. Seismol. Soc. Am.*, *85*, 1127–1143.

Gerolymos, N., and G. Gazetas (2007), A model for grain-crushing-induced landslides–Application to Nikawa, Kobe 1995, *Soil. Dyn. Earthquake Eng.*, *27*, 803–817, doi:10.1016/j.soildyn.2007.01.003.

Gruppo di Lavoro (2004), Redazione della Mappa di Pericolosità Sismica prevista dall'Ordinanza del 20/03/2003, 3274 All.1, 65 pp., 5 annexes, Dip. di Prot. Civ., INGV, Rome, April.

Guadagno, F. M., S. Martino, and G. Scarascia Mugnozza (2003), Influence of man-made cuts on the stability of pyroclastic covers (Campania–southern Italy): A numerical modelling approach, *Environ. Geol.*, *43*, 371–384.

Harp, E. L., and R. C. Wilson (1995), Shaking intensity thresholds for rock falls and slides: Evidence from 1987 Whittier Narrows and Superstition Hills earthquake strong-motion records, *Bull. Seismol. Soc. Am.*, *85*, 1739–1757.

Haskell, N. A. (1962), Crustal reflections of the plane P and SV waves, *J. Geophys. Res.*, *67*, 4751–4767, doi:10.1029/JZ067i012p04751.

Havenith, H. B., D. Jongmans, E. Faccioli, K. Abdrakhmatov, and P. Y. Bard (2002), Site effect analysis around the seismically induced Ananevo rockslide, Kyrgyzstan, *Bull. Seismol. Soc. Am.*, *92*(8), 3190–3209, doi:10.1785/0120010206.

Havenith, H. B., M. Vanini, D. Jongmans, and E. Faccioli (2003a), Initiation of earthquake-induced slope failure: Influence of topographical and other site specific amplification effects, *J. Seismol.*, *7*, 397–412, doi:10.1023/A:1024534105559.

Havenith, H. B., A. Strom, D. Jongmans, K. Abdrakhmatov, D. Delvaux, and P. Tréfois (2003b), Seismic triggering of landslides, part A: Field evidence from the northern Tien Shan, *Nat. Hazards Earth Syst. Sci.*, *3*, 135–149.

Hutchinson, J. N. (1987), Mechanism producing large displacements in landslides on pre-existing shears, *Mem. Soc. Geol. China*, *9*, 175–200.

Hutchinson, J. N., and M. Del Prete (1985), Landslide at Calitri, southern Apennines, reactivated by the earthquake of 23rd November 1980, *Geol. Appl. Idrogeol.*, *XX*(1), 9–38.

Istituto Nazionale di Geofisica e Vulcanologia (2000), *Catalogue of strong Italian earthquakes from 461 a.C. to 1997*, *Publ. CFTI3*, Storia Geofis. Ambiente, Bologna, Italy.

Istituto Nazionale di Geofisica e Vulcanologia (2004), *Catalogo Parametrico dei Terremoti Italiani dal 217 a.C. al 2002*, edited by P. Gasperini et al., *Publ. CPTI04*, Rome. (Available at http://emidius.mi.ingv.it/CPTI04/)

ITASCA Consulting Group (2005), FLAC 5.0: User manual, Licence number 213-039-0127-16143, Earth Sci. Dep., Sapienza–Univ. of Rome, Rome.

Jibson, R. W. (1993), Predicting earthquake-induced landslide displacements using Newmark's sliding block analysis, in *Transportation Research Record*, *1411*, pp. 9–17, Transp, Res. Board, Natl. Res. Counc., Washington, D. C.

Jibson, R. W., E. L. Harp, and J. A. Michael (1998), A method for producing digital probabilistic seismic landslide hazard maps: An example from the Los Angeles, California, area, *U. S. Geol. Surv. Open File Rep.*, *1978*, 98–113.

Jibson, R. W., E. L. Harp, and J. A. Michael (2000), A method for producing digital probabilistic seismic landslide hazard maps, *Eng. Geol. Amsterdam*, *58*, 271–289, doi:10.1016/S0013-7952(00)00039-9.

Keefer, D. K. (1984), Landslides caused by earthquakes, *Geol. Soc. Am. Bull.*, *95*, 406–421, doi:10.1130/0016-7606(1984)95<406:LCBE>2.0.CO;2.

Keefer, D. K. (Ed.) (1998), The Loma Prieta, California Earthquake of October 17, 1989: Landslides, *U.S. Geol. Surv. Prof. Pap.*, *1551-C*.

Keefer, D. K., and R. C. Wilson (1989), Predicting earthquake–induced landslides, with emphasis on arid and semi–arid environments, in *Landslides in a Semi–Arid Environment, Publ.*, vol. 2, edited by D. M. Sadler and D. M. Morton, pp. 118–149, Inland Geol. Soc., Riverside, Calif.

Kuhlemeyer, R. L., and J. Lysmer (1973), Finite element method accuracy for wave propagation problems, *J. Soil Mech. Found. Div. Am. Soc. Civ. Eng.*, *99*(SM5), 421–427.

Lachet, C., M. Bouchon, N. Theodulidis, and P. Y. Bard (1995), Horizontal to vertical spectral ratio and geological conditions, in *Earthquake Engineering: Proceedings of the* 10th *European Conference, Vienna, Austria, 28 August–2 September 1994*, edited by G. Duma, pp. 285–289, A. A. Balkema, Rotterdam, Netherlands.

Lanzo, G. (1993), Deformazione di soglia lineare dei terreni naturali da prove di colonna risonante, Gruppo Naz. di Coordinamento per gli Studi di Ingegneria Geotecnica, *Att. Conv. Ric. Anno*, *1992–93*, 381–384.

Lefebvre, G., D. LeBoeuf, P. Hornych, and L. Tanguay (1992), Slope failures associated with the 1988 Saguenay earthquake, Quebec, Canada, *Can. Geotech. J.*, *26*(1), 162–164.

Li, Y., and J. E. Vidale (1996), Low-velocity fault zone guided waves: Numerical investigations of trapping efficiency, *Bull. Seismol. Soc. Am.*, *86*(2), 371–378.

Li, Y., P. Leary, K. Aki, and P. Malin (1990), Seismic trapped modes in the Oroville and San Andreas fault zones, *Science*, *249*, 763–766, doi:10.1126/science.249.4970.763.

Liu, H. P., D. L. Anderson, and H. Kanamori (1976), Velocity dispersion due to anelasticity: Implications for seismology and mantle composition, *Geophys. J. R. Astron. Soc.*, *47*, 41–58.

Luzi, L., and F. Pergalani (1996), Application of statistical and GIS techniques to slope instability zonation (1:50.000 Fabriano geological map sheet), *Soil. Dyn. Earthquake Eng.*, *15*, 83–94, doi:10.1016/0267-7261(95)00031-3.

Luzi, L., and F. Pergalani (2000), A correlation between slope failures and accelerometric parameters: The 26th September 1997 earthquake (Umbria-Marche, Italy), *Soil. Dyn. Earthquake Eng.*, *20*, 301–313, doi:10.1016/S0267-7261(00)00063-4.

Martino, S., and G. Scarascia Mugnozza (2005), The role of the seismic trigger in the Calitri landslide (Italy): Historical reconstruction and dynamic analysis, *Soil. Dyn. Earthquake Eng.*, *25*, 933–950, doi:10.1016/j.soildyn.2005.04.005.

Martino, S., A. Minutolo, A. Paciello, A. Rovelli, G. Scarascia Mugnozza, and V. Verrubbi (2006), Seismic microzonation of jointed rock-mass

ridges through a combined geomechanical and seismometric approach, *Nat. Hazards*, *39*, 419–449, doi:10.1007/s11069-006-0001-2.

Martino, S., A. Paciello, T. Sadoyan, and G. Scarascia Mugnozza (2007), Dynamic numerical analysis of the giant Vokhchaberd landslide (Armenia), in *Earthquake Geotechnical Engineering: 4th International Conference on Earthquake Geotechnical Engineering-Invited Lect. Ser. Geotech. Geol. Earthquake Eng.*, vol. 6, edited by K. D. Pitilakis Paper Springer, New York.

McCrink, T. P., and C. R. Real (1996), Evaluation of the Newmark method for mapping earthquake-induced landslide hazards in the Laurel 7.5 Quadrangle, Santa Cruz County, California, *Final Tech. Rep. Award 1434-93-G 2334*, 32 pp. U. S. Geol. Surv., Menlo Park, Calif.

Meric, O., S. Garambois, D. Jongmans, M. Wathelet, J. L. Chatelain, and J. M. Vengeon (2005), Application of geophysical methods for the investigations of the large gravitational mass movement of Sechilienne, France, *Can. Geotech. J.*, *42*, 1105–1115, doi:10.1139/t05-034.

Nakamura, Y. (1989), A method for dynamic characteristics estimation of subsurface using microtremor on the ground surface, *Q. Rep. RTRI*, *30*(1), 25–33.

Newmark, N. M. (1965), Effects of earthquakes on dams and embankments, *Geotechnique*, *15*, 139–160.

Norton, J. A., A. B. King, D. K. Bull, H. E. Chapman, G. H. McVerry, T. J. Larkin, and K. C. Spring (1994), Northridge earthquake reconnaissance report: Report of the NZNSEE Reconnaissance Team on the 17 January 1994 Northridge, Los Angeles earthquake, *Bull. N. Z. Natl. Soc. Earthquake Eng.*, *27*(4), 235–344.

Olivares, L. (1996), Caratterizzazione dell'argilla di Bisaccia in condizioni monotone, cicliche e dinamiche e riflessi sul comportamento del "Colle" a seguito del terremoto del 1980, Ph.D. thesis, Univ. degli Studi di Napoli Federico II, Naples, Italy.

Olivares, L., and F. Silvestri (2001), Laboratory and numerical investigation on a post-seismic induced settlement in southern Italy, in *Fourth International Conference on Recent Advances in Geotechnical Engineering and Soil Dynamics* [CD-ROM], edited by S. Prakash, Univ. of Missouri-Rolla, Rolla.

Patacca, E., P. Scandone, M. Bellatalla, N. Perilli, and U. Santini (1992), La zona di giunzione tra l'arco appenninico meridionale nell'Abruzzo e nel Molise, *Studi Geol. Camerti, Spec. Vol.*, *1991/2*(CROP, 11), 417–441.

Pepe, G. (1806), *Ragguaglio istorico-fisico del tremuoto accaduto nel Regno di Napoli la sera de' 26 luglio 1805*, Naples, Italy.

Prestininzi, A., and R. Romeo (2000), Earthquake-induced ground failures in Italy, *Soil. Dyn. Earthquake Eng.*, *58*, 387–397.

Rodriguez, C. E., J. J. Bommer, and R. J. Chandler (1999), Earthquake-induced landslides: 1980–1997, *Soil. Dyn. Earthquake Eng.*, *18*, 325–346, doi:10.1016/S0267-7261(99)00012-3.

Romeo, R. (2000), Seismically induced landslide displacements: A predictive model, *Eng. Geol. Amsterdam*, *58*(3–4), 337–351, doi:10.1016/S0013-7952(00)00042-9.

Rovelli, A., A. Caserta, F. Marra, and V. Ruggiero (2002), Can seismic waves be trapped inside an inactive fault zone? The case study of Nocera Umbra, Central Italy, *Bull. Seismol. Soc. Am.*, *92*(6), 2217–2232, doi:10.1785/0120010288.

Santoni, D., C. Giuffrida, V. Ruggiero, A. Caserta, and P. Lanucara (2004), Web user-friendly interface to produce input data for numerical simulations of seismic wave propagation problem, *Geophys. Res. Abstr.*, *6*, 06,020.

Sarconi, M. (1784), Istoria de' fenomeni del Tremoto avvenuto nelle Calabrie, e nel Valdemone nell'anno 1783. *Posta in luce dalla Reale Accademia delle Scienze, e delle Belle Lettere di Napoli, Ivi, Giuseppe* Campo.

Sassa, K. (1996), Prediction of earthquake induced landslides, in *Landslides: Proceedings of the 7th International Symposium on Landslides*, edited by K. Senneset, pp. 115–132, A. A. Balkema, Rotterdam, Netherlands.

Sassa, K., H. Fukuoka, G. Scarascia Mugnozza, and S. G. Evans (1996), Earthquake-induced landslides: Distribution, motion and mechanisms, *Soils Found.*, 53–64, spec. vol.

Sassa, K., H. Fukuoka, F. Wang, and G. Wang (2005), Dynamic properties of earthquake-induced large-scale rapid landslides within past landslide masses, *Landslides*, *2*, 125–134, doi:10.1007/s10346-005-0055-3.

Savage, W. Z., and W. K. Smith (1986), A model for the plastic flow of landslide, *U. S. Geol. Surv. Prof. Pap.*, *1385*, 32 pp.

Savage, W. Z., and J. Wasowski (2006), A plastic flow model for the Acquara-Vadocello landslide in Senerchia (Southern Italy), *Eng. Geol. Amsterdam*, *83*, 4–21, doi:10.1016/j.enggeo.2005.06.024.

Schnabel, P. B., J. Lysmer, and H. B. Seed (1972), SHAKE: A computer program for earthquake response analysis of horizontally layered sites, *Rep. EERC-72-12*, *Earthquake Eng. Res. Cent.*, Univ. of Calif., Berkeley.

Seed, H. B. (1968), The Fourth Terzaghi lecture: Landslide during earthquakes due to soil liquefaction, *J. Soil Mech. Found. Eng. Div. Am. Soc. Civ. Eng.*, *94*(5), 1055–1122.

Seed, H. B. (1979), Soil liquefaction and cyclic mobility evaluation for level ground during earthquakes, *J. Geotech. Engineer. Div., Am. Soc. Civ. Eng.*, *105*(GT2), 102–155.

Seed, H. B., and I. M. Idriss (1969), Influence of soil conditions on ground motion during earthquakes, *J. Soil Mech. Found. Div. Am. Soc. Civ. Eng.*, *95*, 99–137.

Seed, H. B., and S. D. Wilson (1967), The Turnagain Heights landslide, Anchorage, *J. Soil Mech. Found. Eng. Div. Am. Soc. Civ. Eng.*, *93*(4), 325–353.

Seed, R. B., S. E. Dickenson, and I. M. Idriss (1991), Principal geotechnical aspects of the 1989 Loma Prieta earthquake, *Soils Found.*, *31*(1), 1–26.

Sieberg, A. (1930), Mercalli-Cancani-Sieberg (MCS) macroseismic scale, in *Geologie der Erdbeben, Hanbuch der Geophysic*, pp. 552–555, Springer, Berlin.

Stark, T. D., and I. A. Contreras (1998), Fourth Avenue landslide during the 1964 Alaskan earthquake, *J. Geotech. Geoenviron. Eng.*, *124*(2), 99–109, doi:10.1061/(ASCE)1090-0241(1998)124:2 (99).

Vallée, M., and F. Di Luccio (2005), Source analysis of the 2002 Molise, southern Italy, twin earthquakes (10/31 and 11/01), *Geophys. Res. Lett.*, *32*, L12309, doi:10.1029/2005GL022687.

Wasowski, J., and V. Del Gaudio (2000), Evaluating seismically induced mass movement hazard in Caramanico Terme (Italy), *Eng. Geol.*, *58*(3–4), 291–311, doi:10.1016/S0013-7952(00)00040-5.

Wieczorek, G. F., R. C. Wilson, and E. L. Harp (1985), Map showing slope stability during earthquakes in San Mateo County, California, *U. S. Geol. Surv. Misc. Invest. Map*, *I-1257-E*, scale 1:62500.

Wilson, R. C., and D. K. Keefer (1985), Predicting areal limits of earthquake-induced landsliding, in *Earthquake Hazards in the Los Angeles Region—An Earth-Science Perspective*, edited by J. I. Ziony, *U. S. Geol. Surv. Prof. Pap.* 1360, 317-345.

F. Bozzano, S. Martino, and G. Scarascia Mugnozza, Department of Earth Sciences, Research Centre for Geological Risks (CERI–Valmontone), University of Rome "Sapienza," Place le A. Moro 5, I-00185, Rome, Italy. (salvatore.martino@uniroma1.it)

L. Lenti, LCPC, 58 Boulevard Lefebvre, F-75732 Paris CEDEX 15, France.

A. Paciello, ENEA, Via Anguillarese 301, I-00060, Santa Maria di Galeria, Rome, Italy.